

Article

A distal enhancer at risk locus 11q13.5 promotes suppression of colitis by T_{reg} cells

<https://doi.org/10.1038/s41586-020-2296-7>

Received: 27 March 2019

Accepted: 10 March 2020

Published online: 13 May 2020

 Check for updates

Rabab Nasrallah^{1,2}, Charlotte J. Imianowski^{1,2,12}✉, Lara Bossini-Castillo³, Francis M. Grant¹, Mikail Dogan⁴, Lindsey Placek⁴, Lina Kozhaya⁴, Paula Kuo^{1,2}, Firas Sadiyah^{1,2}, Sarah K. Whiteside^{1,2}, Maxwell R. Mumbach⁵, Dafni Glino³, Panagiota Vardaka^{1,2}, Carly E. Whyte¹, Teresa Lozano¹, Toshitsugu Fujita^{6,7}, Hodaka Fujii^{6,7}, Adrian Liston¹, Simon Andrews⁸, Adeline Cozzani⁹, Jie Yang^{1,2}, Suman Mitra⁹, Enrico Lugli¹⁰, Howard Y. Chang⁵, Derya Unutmac⁴, Gosia Trynka^{3,11}✉ & Rahul Roychoudhuri^{1,2}✉

Genetic variations underlying susceptibility to complex autoimmune and allergic diseases are concentrated within noncoding regulatory elements termed enhancers¹. The functions of a large majority of disease-associated enhancers are unknown, in part owing to their distance from the genes they regulate, a lack of understanding of the cell types in which they operate, and our inability to recapitulate the biology of immune diseases *in vitro*. Here, using shared synteny to guide loss-of-function analysis of homologues of human enhancers in mice, we show that the prominent autoimmune and allergic disease risk locus at chromosome 11q13.5^{2–7} contains a distal enhancer that is functional in CD4⁺ regulatory T (T_{reg}) cells and required for T_{reg}-mediated suppression of colitis. The enhancer recruits the transcription factors STAT5 and NF-κB to mediate signal-driven expression of *Lrrc32*, which encodes the protein glycoprotein A repetitions predominant (GARP). Whereas disruption of the *Lrrc32* gene results in early lethality, mice lacking the enhancer are viable but lack GARP expression in Foxp3⁺ T_{reg} cells, which are unable to control colitis in a cell-transfer model of the disease. In human T_{reg} cells, the enhancer forms conformational interactions with the promoter of *LRRK32* and enhancer risk variants are associated with reduced histone acetylation and GARP expression. Finally, functional fine-mapping of 11q13.5 using CRISPR-activation (CRISPRa) identifies a CRISPRa-responsive element in the vicinity of risk variant rs11236797 capable of driving GARP expression. These findings provide a mechanistic basis for association of the 11q13.5 risk locus with immune-mediated diseases and identify GARP as a potential target in their therapy.

Genetic polymorphisms at human chromosome 11q13.5 are associated with susceptibility to Crohn's disease and ulcerative colitis^{2,3}, type I diabetes⁴, asthma^{5,6}, allergic rhinitis⁶ and atopic dermatitis^{6,7}. The molecular basis for this association is unresolved. Lymphocytes have a critical role in immune-mediated diseases. Imputation of linkage disequilibrium at 11q13.5 revealed a cluster of highly linked variants associated with immune disease occupying an intergenic region not containing the promoters of known protein-coding genes (Fig. 1a, Extended Data Fig. 1). However, examination of histone modifications in multiple primary lymphocyte lineages revealed enrichment of K27-acetylated histone H3 (H3K27ac) at the identified locus in CD4⁺CD127[−]CD25⁺ T_{reg} cells compared with other lineages examined⁸

(Fig. 1b, Extended Data Fig. 2), suggesting the presence of a distal enhancer at 11q13.5 that is active in T_{reg} cells.

Whereas conventional T (T_{conv}) cells promote immune activation and can drive immune-mediated pathology, T_{reg} cells suppress their function to maintain immune homeostasis^{9,10}. T_{reg} cells, which are dependent on the transcription factor Foxp3, exert multiple biological functions that are poorly recapitulated *in vitro*. To better understand the function of the identified locus, we investigated whether a homologous region in mice is amenable to loss-of-function analysis *in vivo*. Analysis of shared synteny between human and mouse genomes identified a region of mouse chromosome 7 homologous to the identified locus in humans (Fig. 1c, d, Supplementary Table 1). This region was accessible

¹Laboratory of Lymphocyte Signalling and Development, The Babraham Institute, Cambridge, UK. ²Department of Pathology, University of Cambridge, Cambridge, UK. ³Immune Genomics Group, Wellcome Sanger Institute, Cambridge, UK. ⁴The Jackson Laboratory, Farmington, CT, USA. ⁵Howard Hughes Medical Institute and Center for Personal Dynamic Regulomes, Stanford University School of Medicine, Stanford, CA, USA. ⁶Chromatin Biochemistry Research Group, Research Institute for Microbial Diseases, Osaka University, Osaka, Japan. ⁷Department of Biochemistry and Genome Biology, Hirosaki University Graduate School of Medicine, Hirosaki, Japan. ⁸Bioinformatics Group, The Babraham Institute, Cambridge, UK. ⁹Inserm UMR1277/CNRS9020, Institut pour la Recherche sur le Cancer de Lille, Lille, France. ¹⁰Humanitas Clinical and Research Center, Milan, Italy. ¹¹Open Targets, Wellcome Genome Campus, Cambridge, UK.

[✉]These authors contributed equally: Rabab Nasrallah, Charlotte J. Imianowski. [✉]e-mail: cji27@cam.ac.uk; gosia@sanger.ac.uk; rr257@cam.ac.uk

Article

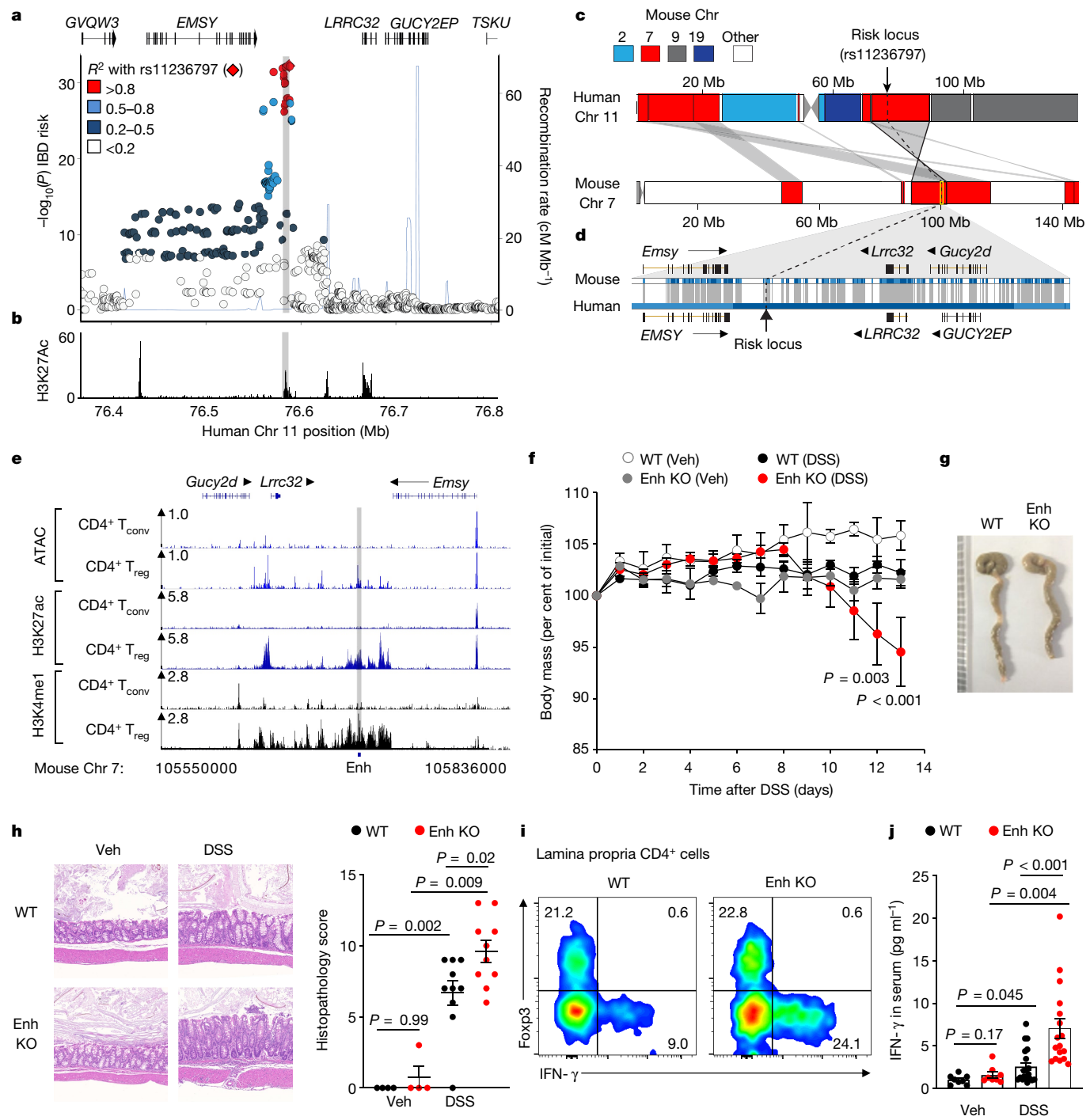


Fig. 1 | A distal intergenic region of mouse chromosome 7 in shared synteny with human 11q13.5 is required to limit gut inflammation. **a**, Association of genetic polymorphisms at 11q13.5 with inflammatory bowel disease (IBD) risk (left axis, genome-wide association study summary statistics and replicate information from ref.²) and imputed recombination rate (right axis; CEU, people of northern European origin from Utah). Shaded area indicates polymorphic risk locus. Points represent individual single nucleotide polymorphisms (SNP; minor allele frequency (MAF) threshold 0.01%). R^2 and MAF calculated using 2,686 genome sequences (from the UK10K project (<https://www.uk10k.org>)). **b**, Alignments showing distribution of H3K27ac at the indicated locus in human CD4⁺CD127⁺CD25⁺T_{reg} cells. Sample information and replicate statistics are in ref.⁸. **c**, Syntenic alignment of indicated human and mouse chromosomes. **d**, Gene-level alignment of mouse and human genome sequences containing the identified risk locus. Grey regions, homology blocks; white spaces, non-aligned in mouse. **e**, Distribution of accessible chromatin (by ATAC-seq) and histone modifications in indicated T cell populations¹¹. Position of putative enhancer (Enh) within the homology

block containing the risk SNP is highlighted in grey. ATAC-seq alignments are representative of three independent biological replicates with samples isolated on different days. **f**, Mass of WT and enhancer-knockout (Enh-KO) mice administered DSS or vehicle (Veh). Difference between daily WT and Enh-KO measurements within each treatment group; two-way ANOVA with Tukey's adjustment for multiple testing. $P > 0.05$, not shown.

g, Representative photographs of large intestines 14 d after initiation of treatment. **h**, Representative haematoxylin and eosin (H&E) staining (left) and combined histopathological colitis scores (right) of large intestines from mice in **g**. **i**, Representative flow cytometry of Foxp3 and IFN- γ expression by CD4⁺ T cells from the large intestinal lamina propria. **j**, Concentration of IFN- γ in the serum of mice in **g**. Representative of three (**f**) and two (**g–i**) independent experiments or pooled from two independent experiments (**j**). In **f**, **h**, $n = 10$ and 4 mice per DSS- and vehicle-treated group. In **j**, $n = 8$ (WT (vehicle)), 8 (Enh-KO (vehicle)), 20 (WT (DSS)) and 17 (Enh-KO). Wilcoxon–Mann–Whitney test (**h**), unpaired two-tailed Student's *t* test (**j**).

Data are mean \pm s.e.m.

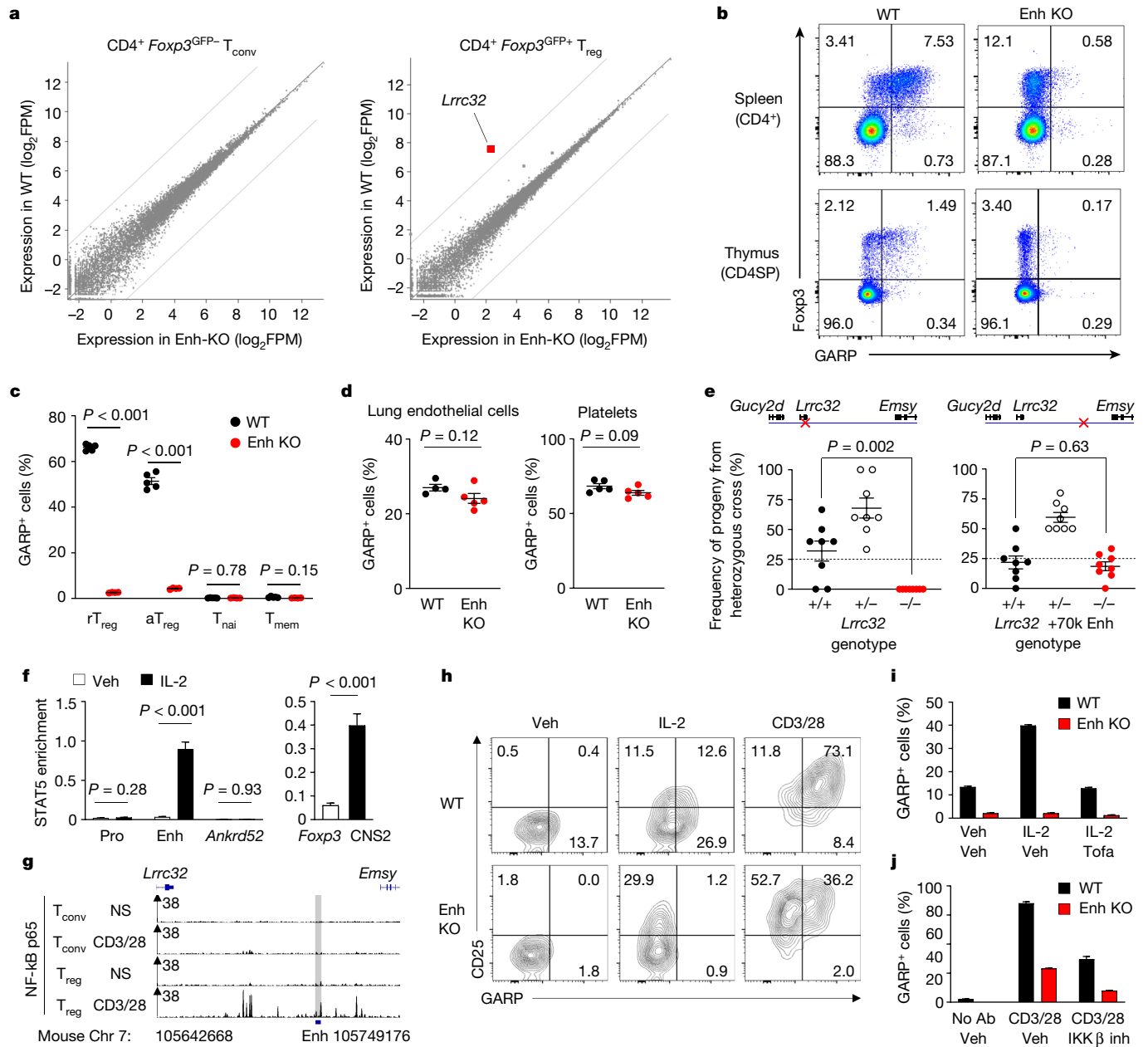


Fig. 2 | *Lrrc32+70k* is required for signal-driven expression of GARP by Foxp3⁺ T_{reg} cells. **a**, Global differences in gene expression between WT and Enh-KO T_{conv} and T_{reg} cells (mean log₂ fragments per million (FPM) from three independent biological replicates, samples isolated on different days). Red dots indicate highly differentially expressed genes ($q < 0.05$, log₂ (fold change) > 5 , mean FPM > 50). Two-tailed Wald test with Benjamini–Hochberg correction. **b**, Flow cytometry of GARP and Foxp3 expression by cells of indicated genotypes. CD4SP, CD4 single positive. **c**, Frequency of GARP⁺ cells within indicated splenic CD4⁺ T cell populations. $n = 5$ (WT) and 4 (Enh-KO). Unpaired two-tailed Student's *t*-test with Bonferroni correction. **d**, GARP expression on CD45⁺CD31⁺ endothelial cells (left; $n = 4$ (WT) and 5 (Enh-KO) mice) and platelets following brief activation ex vivo (right; $n = 5$ mice per group). **e**, Frequency of progeny genotypes after mating of mice heterozygous for the *Lrrc32*-KO (left) or *Lrrc32+70k* Enh-KO alleles (right). Horizontal line indicates expected Mendelian frequency of homozygous offspring. $n = 8$ litters per allele from independent matings. **f**, Input-normalized STAT5-chromatin immunoprecipitation with PCR enrichment at the indicated loci. **g**, NF-κB p65 binding in the indicated cell types with or without TCR stimulation. Sample information and replicate statistics are in ref.²². **h**, CD25 and GARP expression in CD4⁺Foxp3⁺ T_{reg} cells cultured under the indicated conditions for 16 h in vitro. **i,j**, Frequency of GARP⁺ cells among Foxp3⁺ T_{reg} Cells following stimulation with IL-2 with or without pre-treatment with the JAK inhibitor tofacitinib (Tofa; **i**) or with CD3 and CD28 antibodies (CD3/28) with or without pre-treatment with an IKK β inhibitor (IKK β inh; **j**). Data show three (**f**) or four (**i-j**) technical replicates per condition. Data are representative of five (**b**) and two (**c,d,g-j**) independent experiments or pooled from two independent experiments (**f**). Unpaired two-tailed Student's *t*-test (**d-f**). Data are mean \pm s.e.m.

indicates expected Mendelian frequency of homozygous offspring. $n = 8$ litters per allele from independent matings. **f**, Input-normalized STAT5-chromatin immunoprecipitation with PCR enrichment at the indicated loci. **g**, NF-κB p65 binding in the indicated cell types with or without TCR stimulation. Sample information and replicate statistics are in ref.²². **h**, CD25 and GARP expression in CD4⁺Foxp3⁺ T_{reg} cells cultured under the indicated conditions for 16 h in vitro. **i,j**, Frequency of GARP⁺ cells among Foxp3⁺ T_{reg} Cells following stimulation with IL-2 with or without pre-treatment with the JAK inhibitor tofacitinib (Tofa; **i**) or with CD3 and CD28 antibodies (CD3/28) with or without pre-treatment with an IKK β inhibitor (IKK β inh; **j**). Data show three (**f**) or four (**i-j**) technical replicates per condition. Data are representative of five (**b**) and two (**c,d,g-j**) independent experiments or pooled from two independent experiments (**f**). Unpaired two-tailed Student's *t*-test (**d-f**). Data are mean \pm s.e.m.

in mouse T_{reg} cells and enriched in H3K4me1 and H3K27ac (Fig. 1e), consistent with the presence of a distal enhancer at this locus¹¹. We generated knockout mice (hereafter referred to as Enh-KO mice) lacking a 2.3-kb region homologous to the human risk locus (Chr7:105,711,382–105,713,753; 71% sequence identity) using CRISPR-based mutagenesis.

Enh-KO mice exhibited similar body mass and survival to wild-type (WT) littermates (Extended Data Fig. 3a,b). The phenotype of T cells in the thymus and periphery were similar between WT and Enh-KO mice (Extended Data Fig. 3c-f). This suggested that the identified enhancer is not required to maintain immune homeostasis under basal conditions.

Susceptibility to complex diseases is a product of genetic and environmental factors. Given the association of 11q13.5 polymorphisms with ulcerative colitis and Crohn's disease^{2,3}, we tested the susceptibility of Enh-KO mice to colitis driven by dextran sulfate sodium (DSS), the severity of which is affected by T_{reg} cells^{12,13}. Enh-KO mice were more susceptible to DSS-induced colitis, as indicated by increased weight loss (Fig. 1f), reduction in colon length (Extended Data Fig. 4a) and induction of macroscopic and histopathological features of colitis (Fig. 1g, h, Extended Data Fig. 4b, c). Greater frequencies of CD4⁺T_{conv} cells within the colonic lamina propria and mesenteric lymph nodes of DSS-treated Enh-KO mice expressed interferon-γ (IFN-γ), whereas there were no differences in the frequency of Foxp3⁺T_{reg} cells (Fig. 1i, Extended Data Fig. 5a). This coincided with increased concentrations of IFN-γ, tumour necrosis factor (TNF) and interleukin-6 (IL-6) in sera of DSS-treated Enh-KO mice (Fig. 1j, Extended Data Fig. 5b, c). By contrast, we noted similar levels of Cys-X-Cys motif ligand 1 (CXCL1) and IL-10 in sera of WT and Enh-KO mice (Extended Data Fig. 5d, e). Collectively, these results indicate that the identified enhancer is required to maintain gut immune homeostasis in the face of extrinsic colitogenic stimuli.

Since the identified region contained active enhancer marks in Foxp3⁺T_{reg} cells, we investigated whether it regulates gene expression in these cells. We analysed CD4⁺T_{reg} and T_{conv} cells isolated by fluorescence-activated cell sorting from WT and Enh-KO Foxp3^{eGFP} reporter mice using massively parallel RNA sequencing (RNA-seq). Whereas enhancer loss did not significantly affect gene expression within T_{conv} cells, its loss in T_{reg} cells resulted in a reduction of approximately 36-fold in the expression of the *Lrrc32* gene, which encodes the protein GARP (Fig. 2a, Supplementary Table 2). Assay for transposase-accessible chromatin using sequencing (ATAC-seq) analysis showed that whereas the enhancer is required for the maintenance of local accessible chromatin, it is not required for maintaining the broader landscape of accessible elements in T_{reg} cells (Extended Data Fig. 6a, b).

GARP is a 72-kDa transmembrane glycoprotein expressed by T_{reg} cells, platelets, endothelial cells and lipopolysaccharide (LPS)-activated B cells^{14–19}. GARP binds latent TGF-β on the cell surface, which is cleaved by integrin-αvβ8 to cause local release of active TGF-β. Consistent with reduced *Lrrc32* expression by T_{reg} cells from Enh-KO mice, flow cytometry analysis revealed marked reduction in expression of GARP on the surface of Foxp3⁺T_{reg} cells in the spleen, thymus and mesenteric lymph nodes of Enh-KO mice (Fig. 2b and Extended Data Fig. 6c, d). By contrast, GARP expression was not substantially reduced on Enh-KO naïve or memory CD4⁺T_{conv} cells isolated ex vivo (Fig. 2c, Extended Data Fig. 7a) or T_{conv} cells stimulated briefly in vitro (Extended Data Fig. 7b). Consistently, we noted the presence of acetylated histones at the identified enhancer in resting and activated T_{reg} cells that was Foxp3-dependent and reduced in naïve and effector CD4⁺T_{conv} cells²⁰ (Extended Data Fig. 7c). Additionally, the enhancer was not required for GARP expression on other cells known to express GARP, including lung endothelial cells, activated platelets and LPS-activated B cells (Fig. 2d, Extended Data Fig. 8a, b), and did not regulate GARP expression on a variety of other splenic non-T_{reg} cell types (Extended Data Fig. 8c–e). Consistent with tissue specificity in the function of the enhancer, whereas homozygous disruption of the *Lrrc32* gene resulted in complete early lethality, viable progeny homozygous for deletion of the enhancer (hereafter *Lrrc32*+70k) were obtained at expected Mendelian ratios (Fig. 2e).

We noted the presence of highly conserved binding motifs for the transcription factors STAT5 and NF-κB within *Lrrc32*+70k; STAT5 and NF-κB have canonical roles in IL-2 and T cell receptor (TCR)-driven gene expression, respectively (Extended Data Fig. 9a). We investigated whether these transcription factors bind *Lrrc32*+70k to mediate signal-driven GARP expression in T_{reg} cells. STAT5 was recruited to *Lrrc32*+70k in response to brief (1h) IL-2 stimulation of in vitro-derived induced T_{reg} (iT_{reg}) cells (Fig. 2f). Correspondingly, we noted STAT5

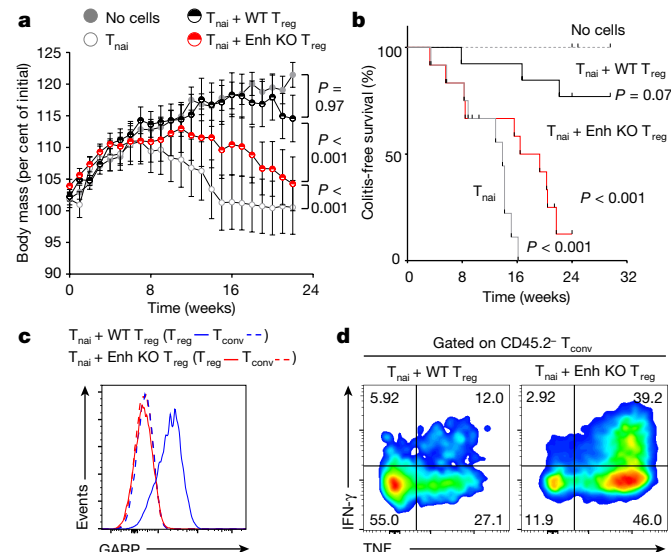


Fig. 3 | *Lrrc32*+70k promotes T_{reg}-mediated suppression of colitis. **a, b**, Body mass (**a**) and colitis-free survival (**b**) of *Rag2*-deficient mice injected with WT naïve CD4⁺CD25[−]CD45RB^{high} T cells alone (T_{nai}; *n* = 12), or in combination with CD4⁺CD25^{high} T_{reg} cells derived from WT (*n* = 13) or Enh-KO (*n* = 12) mice. Control mice did not receive cells (*n* = 10). **c**, GARP expression, gated on the indicated cells from mesenteric lymph nodes of mice euthanized 100 d following reconstitution. T_{reg}, CD45.2⁺ cells; T_{conv}, CD45.2[−] cells. **d**, Representative flow cytometry of expression of indicated cytokines by CD45.2⁺ cells from mesenteric lymph nodes following brief restimulation ex vivo. Pooled results from two independent experiments (**a, b**). Data are representative of two independent experiments (**c, d**). Two-way ANOVA with Tukey's correction for multiple comparisons (**a**) and Mantel–Cox log-rank test (**b**). Data are mean \pm s.e.m.

binding at the homologous enhancer in human T_{reg} cells but not T_{conv} cells²¹ (Extended Data Fig. 9b). Analysis of known NF-κB p65 binding activity also revealed TCR-driven NF-κB p65 binding to *Lrrc32*+70k in T_{reg} cells but not in T_{conv} cells, in response to TCR stimulation²² (Fig. 2g). Consistent with its ability to bind signal-dependent transcription factors, there was an absolute requirement of *Lrrc32*+70k for IL-2-driven GARP expression in T_{reg} cells, whereas TCR-driven GARP expression was only partially enhancer-dependent (Fig. 2h, Extended Data Fig. 9c). IL-2-driven GARP expression was abrogated by pre-treatment of cells with the JAK inhibitor Tofacitinib, which inhibits signal-driven activation of STAT transcription factors²³ (Fig. 2i). Similarly, GARP induction driven by TCR stimulation was partially blocked by pre-treatment of cells with BI 605906, a highly specific inhibitor of the protein kinase IKKβ, the activity of which is required for canonical NF-κB activation (Fig. 2j). This result is consistent with previous RNA-seq analyses of WT and Rela^{−/−}Rel^{−/−} T_{reg} cells, which demonstrated markedly decreased stimulation-driven expression of *Lrrc32* mRNA in the absence of canonical NF-κB signalling²². Collectively, these data demonstrate that *Lrrc32*+70k binds to STAT5 and NF-κB in response to IL-2 and TCR signalling and functions as a regulatory node for signal-driven GARP expression in T_{reg} cells.

Because Enh-KO mice exhibited increased susceptibility to colitis, we investigated whether T_{reg} cells from Enh-KO mice are defective in their ability to control gut inflammation. GARP is dispensable for the suppressive function of mouse T_{reg} cells as measured in vitro²⁴, but is required for optimal suppression of colitis in vivo^{25,26}. To test the function of Enh-KO T_{reg} cells in vivo, we reconstituted *Rag2*-deficient mice with 4×10^5 CD4⁺ naïve T cells from WT mice, alone or in combination with 1×10^5 WT or Enh-KO T_{reg} cells. Whereas weight loss and induction of clinical features of colitis caused by transfer of naïve T cells were reduced by the co-transfer of WT T_{reg} cells, T_{reg} cells from Enh-KO

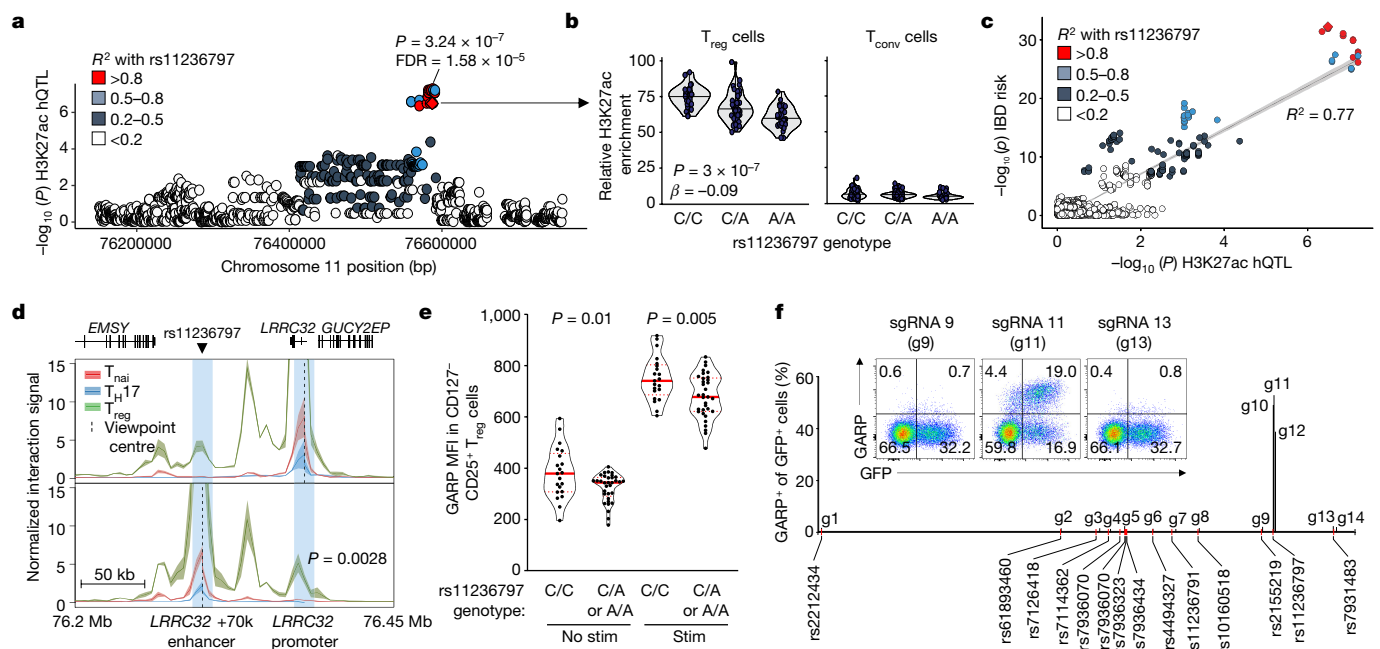


Fig. 4 | Inflammatory bowel disease risk alleles at 11q13.5 affect enhancer histone acetylation and GARP expression in human CD4⁺ T_{reg} cells.

a, Histone quantitative trait locus (hQTL) analysis of the association between indicated SNP (points) and histone H3K27ac enrichment at the identified enhancer at chr11:76586431–76600121 in human CD4⁺CD127⁻CD25⁺T_{reg} cells; $n = 91$ donors. Nominal P and false discovery rate (FDR) of the most significantly associated SNP are shown. **b**, Association of rs11236797 polymorphisms with H3K27ac enrichment at chr11:76586431–76600121 in human T_{reg} and CD4⁺T_{conv} cells²⁷; $n = 91$ donors. **c**, Colocalization of the association of indicated SNP with H3K27ac enrichment (x-axis) and inflammatory bowel disease risk (y-axis). Colocalization posterior probability = 0.97; $n = 91$ donors. **d**, Reciprocal v4C analysis of H3K27ac-enriched HiChIP interactions in human CD4⁺ naive, T_{reg} and

T_{H17} cells²⁸. Graph lines and shaded area show mean and s.e.m.; $n = 3$ biological replicates. **e**, GARP mean fluorescence intensity (MFI) in CD127⁻CD25⁺T_{reg} cells from donors of indicated rs11236797 genotypes stimulated with CD3 and CD28 antibodies and IL-2 (stim) or medium only (no stim). $n = 21$ (C/C) and 33 (C/A or A/A) donors. **f**, GARP expression in human GFP⁺ (transduced) CD4⁺ T cells expressing sgRNAs targeting dCas9–VP64 to loci indicated by the x-axis position of bars. Positions of risk SNP are shown. Representative of three independent experiments using cells from three different donors. Linear regression; two-sided (**a–c**) or unpaired two-tailed (**d, e**) Student's *t* test. In violin plots, lines show median and interquartile range and outlines show frequency distribution.

mice were insufficient to suppress colitis (Fig. 3a, b). Distinguishing transferred CD45.2⁺ T_{conv} cells from CD45.2⁺ T_{reg} cells, we found that Enh-KO T_{reg} cells accumulated at higher frequencies than WT T_{reg} cells in mesenteric lymph nodes of recipient mice (Extended Data Fig. 9d), but expressed substantially reduced GARP in both mesenteric lymph nodes and spleen (Fig. 3c, Extended Data Fig. 9e). Consistent with their inability to adequately constrain colitis, we observed increased effector cytokine expression by CD45.2⁺ T_{conv} cells among mice that received Enh-KO T_{reg} cells (Fig. 3d, Extended Data Fig. 9f). Collectively, these data indicate that Lrrc32 +70k is required for T_{reg}-mediated suppression of colitis *in vivo*.

We next tested whether genetic variations at 11q13.5 affect enhancer function in human T_{reg} cells. We measured H3K27ac enrichment in CD4⁺CD127⁻CD25⁺T_{reg} cells isolated by fluorescence-activated cell sorting (FACS) from peripheral blood of genotyped healthy donors. We found that a cluster of linked 11q13.5 variants was associated with differential enhancer acetylation in human T_{reg} cells²⁷ (Fig. 4a, b, Supplementary Tables 3–4). Notably, there was significant colocalization between variants associated with differential acetylation and those associated with increased risk of inflammatory bowel disease (Fig. 4c and Supplementary Table 5). Reciprocal virtual 4C (v4C) analysis of previously generated H3K27ac HiChIP interaction maps²⁸ revealed significant interactions between the identified enhancer and the LRRC32 promoter within human T_{reg} but not naive or T_{H17} cells (Fig. 4d), contained within a sub-topologically associated domain previously mapped within a human lymphoid line²⁹ (Extended Data Fig. 10a, b). To test the effect of 11q13.5 polymorphisms on LRRC32 expression, CD4⁺CD127⁻CD25⁺T_{reg} cells were sorted by FACS from peripheral blood

of genotyped healthy donors and LRRC32 expression was determined using RNA-seq. This analysis revealed that 11q13.5 polymorphisms were nominally associated with differential LRRC32 mRNA expression under basal conditions (Extended Data Fig. 10c). Moreover, rs11236797 polymorphisms were significantly associated with both basal and stimulation-driven GARP expression on CD4⁺CD127⁻CD25⁺T_{reg} cells (Fig. 4e). Thus, disease-associated genetic polymorphisms within 11q13.5 affect enhancer histone acetylation and GARP expression on human T_{reg} cells.

Since risk variants at 11q13.5 are in high linkage disequilibrium, we performed a CRISPR-activation (CRISPRa) screen to enable fine-mapping of candidate stimulation-responsive enhancers and causal variants³⁰ within 11q13.5. Single guide RNA (sgRNA) target sequences in proximity to risk variants within 11q13.5 were subcloned into lentiviral vectors and individually co-expressed with VP64 fused to endonuclease-dead Cas9 (dCas9–VP64) and GFP, and activator helper complex MS2–P65–HSF1 in primary *in vitro*-stimulated human CD4⁺ T cells (Supplementary Table 6). Expression of GARP on the surface of GFP⁺ (transduced) cells was measured; of 14 sgRNAs tested, three sgRNAs in the proximity of rs11236797 strongly induced GARP expression (Fig. 4f), indicating the presence of a CRISPRa-responsive element in the vicinity of risk variant rs11236797 with the capacity to drive GARP expression.

Genome-wide association studies have provided insights into the genetic architecture of human immune-mediated disease. However, in many cases, it has been difficult to infer the cell types underlying disease pathophysiology. In this study, we find that the prominent risk locus for autoimmune or allergic disease at human chromosome 11q13.5 contains a distal enhancer that is required to control signal-driven expression

Article

of GARP by T_{reg} cells. Using shared synteny to guide loss-of-function analysis of the homologous enhancer in mice, we find that this function is required to promote T_{reg}-mediated suppression of colitis. These findings provide a basis for association of 11q13.5 polymorphisms with susceptibility to complex autoimmune and allergic diseases and identify GARP as a potential therapeutic target.

Online content

Any methods, additional references, Nature Research reporting summaries, source data, extended data, supplementary information, acknowledgements, peer review information; details of author contributions and competing interests; and statements of data and code availability are available at <https://doi.org/10.1038/s41586-020-2296-7>.

1. Maurano, M. T. et al. Systematic localization of common disease-associated variation in regulatory DNA. *Science* **337**, 1190–1195 (2012).
2. de Lange, K. M. et al. Genome-wide association study implicates immune activation of multiple integrin genes in inflammatory bowel disease. *Nat. Genet.* **49**, 256–261 (2017).
3. Anderson, C. A. et al. Meta-analysis identifies 29 additional ulcerative colitis risk loci, increasing the number of confirmed associations to 47. *Nat. Genet.* **43**, 246–252 (2011).
4. Onengut-Gumuscu, S. et al. Fine mapping of type 1 diabetes susceptibility loci and evidence for colocalization of causal variants with lymphoid gene enhancers. *Nat. Genet.* **47**, 381–386 (2015).
5. Ferreira, M. A. et al. Identification of IL6R and chromosome 11q13.5 as risk loci for asthma. *Lancet* **378**, 1006–1014 (2011).
6. Ferreira, M. A. et al. Shared genetic origin of asthma, hay fever and eczema elucidates allergic disease biology. *Nat. Genet.* **49**, 1752–1757 (2017).
7. Paternoster, L. et al. Meta-analysis of genome-wide association studies identifies three new risk loci for atopic dermatitis. *Nat. Genet.* **44**, 187–192 (2012).
8. Kundaje, A. et al. Integrative analysis of 111 reference human epigenomes. *Nature* **518**, 317–330 (2015).
9. Sakaguchi, S., Yamaguchi, T., Nomura, T. & Ono, M. Regulatory T cells and immune tolerance. *Cell* **133**, 775–787 (2008).
10. Josefowicz, S. Z., Lu, L. F. & Rudensky, A. Y. Regulatory T cells: mechanisms of differentiation and function. *Annu. Rev. Immunol.* **30**, 531–564 (2012).
11. Kitagawa, Y. et al. Guidance of regulatory T cell development by Satb1-dependent super-enhance establishment. *Nat. Immunol.* **18**, 173–183 (2017).
12. Boschetti, G. et al. Gut inflammation in mice triggers proliferation and function of mucosal Foxp3⁺ regulatory t cells but impairs their conversion from CD4+ T cells. *J. Crohn's Colitis* **11**, 105–117 (2017).
13. Worthington, J. J. et al. Integrin avB8-mediated TGF-β activation by effector regulatory T cells is essential for suppression of T-cell-mediated inflammation. *Immunity* **42**, 903–915 (2015).
14. Tran, D. Q. et al. GARP (LRRC32) is essential for the surface expression of latent TGF-β on platelets and activated FOXP3⁺ regulatory T cells. *Proc. Natl. Acad. Sci. USA* **106**, 13445–13450 (2009).
15. Wang, R., Wan, Q., Kozhaya, L., Fujii, H. & Unutmaz, D. Identification of a regulatory T cell specific cell surface molecule that mediates suppressive signals and induces Foxp3 expression. *PLoS ONE* **3**, e2705 (2008).
16. Dedobbeleer, O., Stockis, J., van der Woning, B., Coulie, P. G. & Lucas, S. Active TGF-β1 released from GARP/TGF-β1 complexes on the surface of stimulated human B lymphocytes increases class-switch recombination and production of IgA. *J. Immunol.* **199**, 391–396 (2017).
17. Wallace, C. H. et al. B lymphocytes confer immune tolerance via cell surface GARP-TGF-β complex. *JCI Insight* **3**, e99863 (2018).
18. Vermeersch, E. et al. The role of platelet and endothelial GARP in thrombosis and hemostasis. *PLoS One* **12**, e0173329 (2017).
19. O'Connor, M. N. et al. Functional genomics in zebrafish permits rapid characterization of novel platelet membrane proteins. *Blood* **113**, 4754–4762 (2009).
20. Arvey, A. et al. Genetic and epigenetic variation in the lineage specification of regulatory T cells. *eLife* **4**, e07571 (2015).
21. Schmidl, C. et al. The enhancer and promoter landscape of human regulatory and conventional T-cell subpopulations. *Blood* **123**, e68–e78 (2014).
22. Oh, H. et al. An NF-κB transcription-factor-dependent lineage-specific transcriptional program promotes regulatory T cell identity and function. *Immunity* **47**, 450–465 (2017).
23. Changelian, P. S. et al. Prevention of organ allograft rejection by a specific Janus kinase 3 inhibitor. *Science* **302**, 875–878 (2003).
24. Edwards, J. P. et al. Regulation of the expression of GARP/latent TGF-β1 complexes on mouse T cells and their role in regulatory T cell and T_H17 differentiation. *J. Immunol.* **190**, 5506–5515 (2013).
25. Eschborn, M. et al. Activated glycoprotein A repetitions predominant (GARP)-expressing regulatory T cells inhibit allergen-induced intestinal inflammation in humanized mice. *J. Allergy Clin. Immunol.* **136**, 159–168 (2015).
26. Salem, M. et al. GARP dampens cancer immunity by sustaining function and accumulation of regulatory T cells in the colon. *Cancer Res.* **79**, 1178–1190 (2019).
27. Chen, L. et al. Genetic drivers of epigenetic and transcriptional variation in human immune cells. *Cell* **167**, 1398–1414 (2016).
28. Mumbach, M. R. et al. Enhancer connectome in primary human cells identifies target genes of disease-associated DNA elements. *Nat. Genet.* **49**, 1602–1612 (2017).
29. Rao, S. S. et al. A 3D map of the human genome at kilobase resolution reveals principles of chromatin looping. *Cell* **159**, 1665–1680 (2014).
30. Simeonov, D. R. et al. Discovery of stimulation-responsive immune enhancers with CRISPR activation. *Nature* **549**, 111–115 (2017).

Publisher's note Springer Nature remains neutral with regard to jurisdictional claims in published maps and institutional affiliations.

© The Author(s), under exclusive licence to Springer Nature Limited 2020

Methods

Mice and reagents

Mice were housed at the Babraham Institute Biological Services Unit and experiments were conducted with the approval of the UK Home Office and the Babraham Institute Animal Welfare and Ethical Review Body and complied with all relevant ethical regulations. *Lrrc32*+70k Enh-KO mice were generated as described below, and were crossed to *Foxp3*^{eGFP} mice (C.Cg-Foxp3tm2Tch/J; Jackson laboratories) to generate WT and Enh-KO *Foxp3*^{eGFP} reporter mice. *Rag2*-deficient mice used as hosts for T cell-transfer colitis experiments (B6 (Cg)-Rag2tm1.1Cgn/J) were originally obtained from Jackson laboratories and maintained at the Babraham Institute. *Lrrc32*^{-/-} mice have been described previously²⁴. Littermate controls or age- and sex-matched mice on a C57BL/6 background were used as indicated. Mendelian ratios of early viability were calculated by assessing the genotypes of all progeny surviving to two weeks of age resulting from heterozygous Enh-KO or *Lrrc32*-KO crosses.

Generation of *Lrrc32*+70k Enh-KO mice

sgRNAs containing the target sequences gRNA1 (AATGAAG GATG-GGCCA CGCTGG) and gRNA2 (TTACTCA CCACCACC ACAAGAGG) and Cas9 mRNA were generated by in vitro transcription and coinjected into fertilized C57BL/6 oocytes which were transferred into pseudopregnant females. The genomic region surrounding the targeted locus was amplified from genomic DNA of resultant founder progeny by PCR using the following primers: 5'-TTATTCTT GGGAACAGG GGCATG-3' and 5'-AGAGGCT ACTTTGTTAC TTGGTCCC-3' and amplicons were sequenced using the following forward primer: 5'-CAATCTG TCAC-CTATCA GCAACGT-3'. Founder progeny bearing a 2,372 base pair (bp) deletion corresponding to base pairs 105711382–105713753 of chromosome 7 (NCBI37/mm9), the centre of which is 69,836 bp downstream of the transcriptional start site of *Lrrc32*, were mated with WT C57BL/6 mice to generate heterozygous F₁ mice which were subsequently intercrossed to generate WT and Enh-KO littermate progeny.

Flow-cytometry analysis of primary tissues

Single-cell suspensions from lymphoid tissues were prepared by dissociating tissues over 40-μm cell strainers. Lungs were minced in medium containing 20 μg/ml DNase I (Roche) and 1 mg/ml collagenase (Sigma-Aldrich) and incubated with agitation at 37 °C for 30 min. Blood from tail veins or terminal cardiac bleeds were isolated in EDTA Microvette tubes (Sarstedt). Erythrocytes were lysed using ice cold ACK Lysing Buffer (Gibco) for 45 s. Cells requiring intracellular staining of cytokines before flow cytometry analysis were stimulated using phorbol 12-myristate 13-acetate (PMA), ionomycin and brefeldin A (BFA) for 4-6 h in complete medium. Viable cells were discriminated by staining with Zombie UV live/dead dye (Biolegend) or eFluor 780 live/dead dye (eBioscience) according to the manufacturer's instructions. Cells were then incubated with specific antibodies for 30 min on ice in the presence of monoclonal antibodies to block FcγR binding (anti-CD16/32 clone 2.4G2, BE0307). For intracellular staining, the eBioscience Foxp3/Transcription Factor Staining Buffer Set (Invitrogen) was used in accordance with the manufacturer's instructions followed by intracellular staining with fluorochrome-conjugated antibodies.

The following fluorochrome-conjugated antibodies against mouse surface and intracellular antigens were used: anti-GARP (clone YGIC86, eBioscience 12-9891-82), anti-FoxP3 (clone FJK-16 s, eBioscience 17-5773-82), anti-CD45.2 (clone 104, eBioscience 69-0454-82), anti-TNF (clone MP-XT22, eBioscience 25-7321-82), anti-IFN-γ (clone XMG1.2, eBioscience 45-7311-82), anti-GL7 (clone GL7, BioLegend 144604), anti-CD25 (clone PC61, Becton Dickinson 564023), anti-CD4 (clone RM4-5, eBioscience 48-0042-82), anti-CD62L (clone MEL-14 BioLegend, 104441), anti-CD44 (clone IM7, eBioscience 55313), anti-CD8a (clone 53-6.7, BD Horizon 563786), anti-CD19 (clone eBio1D3, eBioscience 17-0193-80), anti-B220 (clone RA3-6B2, eBioscience 103236).

The following fluorochrome-conjugated antibodies against human surface and intracellular antigens were used: anti-CD3 (clone UCHT1, BD Horizon 563546), anti-CD4 (clone SK3, BioLegend 344608), anti-CD127 (clone A019D5, BioLegend 351320), anti-CD25 (clone BC96, BioLegend 302632), anti-GARP (clone G14D9, eBioscience 12-9882-42). Data were acquired using BD Fortessa or LSRII flow cytometers and analysed using FlowJo (TreeStar).

For high parameter flow cytometry, cells were incubated on ice for 30 min in the presence of 2.4G2 monoclonal antibodies to block FcγR binding. Cells were then stained with Fixable Viability Dye eFlour 780 and antibodies against surface antigens, followed by fixation with 2% formaldehyde and staining with antibodies against intracellular antigens. Antibodies used were anti-γδ-TCR clone GL3 (eBioscience), anti-CD11b clone M1/70 (eBioscience), anti-CD90.2 clone 53-2.1 (Biolegend), anti-CD11c clone N418 (Biolegend), anti-Ly6G clone 1A8 (Biolegend), anti-Ly6C clone HK1.4 (Biolegend), anti-Foxp3 clone FJK-16 s (eBioscience), anti-Siglec F clone E50-2440 (BD Biosciences), anti-TCRβ clone H57-597 (BD Bioscience), anti-GARP clone YGIC86 (eBioscience), anti-F4/80 clone BM8 (eBioscience), anti-NK1.1 clone PK136 (Biolegend), anti-CD3 clone 145-2C11 (eBioscience), anti-CD45 clone 30-F11 (BD Biosciences), anti-CD4 clone GK1.5 (BD Biosciences), anti-CD19 clone 1D3 (BD Biosciences), anti-PDCA-1 clone 927 (BD Biosciences), anti-CD8α clone 53-6.7 (eBioscience), anti-MHCII (I-A/I-E) clone M5/114.15.2 (eBioscience). Samples were acquired on a Propel Labs YETI/Bio-Rad ZE5 and analysed using FlowJo (TreeStar).

Analysis of platelets. Whole mouse blood was collected into microcentrifuge tubes containing 100 μl HEPES medium (132 mM NaCl, 6 mM KCl, 1 mM MgSO₄, 20 mM HEPES and 5 mM glucose) as previously described³¹. Samples were diluted 2× in HEPES medium, and then centrifuged at room temperature for 15 min at 100g. Platelet rich plasma was incubated for 15 min at room temperature in 100 μl of HEPES medium containing the following antibodies: anti-CD45.2, anti-CD31, anti-CD9, anti-GARP and anti-Ter119 (eBioscience) before flow cytometry analysis. Data were acquired using BD Fortessa flow cytometers and analysed using FlowJo (TreeStar).

Cell culture stimulation assays

Total CD4⁺ T cells were isolated from single-cell spleen suspensions using magnetic negative selection (eBioscience). Cells were stimulated at 37 °C, 5% CO₂ for 16 h in RPMI culture medium supplemented with 10% fetal calf serum (Sigma), 1% penicillin and streptomycin (pen/strep; Gibco), and 50 μM β-mercaptoethanol, non-essential amino acids (Gibco) and Glutamax (Gibco). Cells were plated at density of 1 × 10⁵ cells per well on 96-well plates in the presence or absence of 10 ng ml⁻¹ recombinant human IL-2 (Peprotech) with or without 300 nM tofacitinib (Sigma) or 10 μM BI605906 (Tocris). Where indicated, plates were coated overnight with 5 μg ml⁻¹ anti-CD3 (clone 145.2C11; BioXcell BE0001-1) and 5 μg ml⁻¹ anti-CD28 (clone 37.51 BioXcell BE0015-1) monoclonal antibodies in PBS before washing and plating of cells for stimulation. Cells were harvested and analysed by flow cytometry. To detect LPS-induced GARP expression on B cells, cells from erythrocyte-lysed blood were stimulated in RPMI complete medium (RPMI, 10% FCS, 1% pen/strep and 50 μM β-mercaptoethanol) containing 0.5 mg ml⁻¹ lipopolysaccharide (Sigma) at 37 °C, 5% CO₂ for 48 h. At the end of the stimulation period, cells were collected and analysed using flow cytometry.

Colitis experiments

Average initial body weights before induction of colitis were calculated from daily body weight measurements over a period of 1–2 weeks before induction of colitis. Colitis experiments were performed in a specialized room within our animal facility with enriched microflora. For DSS colitis experiments, mice were treated with 2% (w/v) DSS (Sigma Aldrich 42867-100g; lot no. BCBW8358 and BCCB5021) in the drinking water for

Article

up to 16 days. Body weight, general appearance, occult or gross blood loss and stool consistency were monitored daily to provide an objective clinical severity score. Mice were euthanized if they had >20% body weight loss or reached a level of clinical severity requiring euthanasia. For analysis of colon length, serum cytokines and gut histopathology, mice were euthanized at 16 days following the initiation of DSS administration and the large intestine was collected. The length of isolated large intestines was measured in a blinded fashion and stored in 10% formaldehyde (Sigma) for subsequent histopathology analysis using H&E staining. Serum samples were also collected from each animal for bead array analysis of serum cytokines. For analysis of cytokine production by T_{conv} mice were euthanized at 13 days following the initiation of DSS administration and the mesenteric lymph node and large intestine were collected. Cytokine expression was measured by flow cytometry after a 4 h period of restimulation with PMA, ionomycin and BFA.

The T cell-transfer colitis model has been described previously³². In brief, $Rag2^{-/-}$ mice were injected intravenously with 4×10^5 FACS-sorted naive CD4 $^+$ CD25 $^-$ CD45RB high cells from WT mice with or without 1×10^5 WT or Enh-KO CD4 $^+$ CD25 high T_{reg} cells. Mice were monitored daily for body weight and clinical signs of colitis from which objective clinical severity scores were assigned (Body weight (0–4), general appearance (0–4), occult or gross blood loss (0–4) and stool consistency (0–4)). Colitis-free survival was calculated by measuring the time following cell transfer until the onset of clinical colitis. Events were determined on the basis of severity (combined objective score ≥ 5 on a given day) or chronicity (total combined score ≥ 48 over the preceding 25 days). Mice were censored if they survived to study end without experiencing a colitis event or if the animal was euthanized for severe non-colitis pathology. Mice were euthanized if they reached 20% body weight loss or a level of clinical severity requiring euthanasia. Sections of large intestine were fixed in buffered 10% formalin and stained with H&E.

Isolation and analysis of large intestinal lamina propria lymphocytes

Lamina propria leukocytes (LPL) were isolated from the large intestine (caecum and colon) using the following method: the tissue was removed, washed and cut into 5-mm-long pieces followed by incubating at room temperature in 10 ml PBS containing 1 μ l of 1 M DTT for 10 min with gentle shaking. The samples were filtered through 70- μ m cell strainers with 10 ml RPMI-2 (RPMI supplemented with 1% HEPES and 2% FCS). The remaining tissues on the strainer were digested twice in 10 ml RPMI-2 with 30 mM EDTA at 230 rpm, 37 °C for 10 min and the filtrate discarded. The remaining tissues were homogenized into small pieces and digested in 6 ml of RPMI-2 containing 0.05 mg ml $^{-1}$ collagenase VIII (Sigma) and 0.15 mg ml $^{-1}$ DNase I (Roche) at 37 °C for 45 min with gentle shaking. The sample was then filtered for density gradient as the LPL sample. Isolated LPL was resuspended in 6 ml 40% Percoll (Sigma) and underlaid with 1 ml 80% Percoll for centrifugation. Centrifugation was carried out without brake at 2,300 rpm for 25 min at room temperature. The interface was extracted, pelleted and resuspended in RPMI-2 for subsequent analysis by flow cytometry.

RNA-seq analysis

CD4 $^+$ *Foxp3* $^{eGFP+}$ T_{reg} and CD4 $^+$ *Foxp3* $^{eGFP-}$ T_{conv} cells were sorted by FACS from WT and Enh-KO *Foxp3* eGFP reporter mice. In brief, total CD4 $^+$ T cells were pre-enriched from single cell spleen suspensions using magnetic negative selection (eBioscience) before FACS-sorting of GFP $^+$ and GFP $^-$ CD4 $^+$ T cells using a BD Influx instrument (Becton Dickinson Biosciences). Cells were sorted into solutions of RPMI1640 medium supplemented with 20% FBS and pellets were stored in RNAlater (Ambion) at -80 °C. Total RNA was extracted using the RNeasy Plus Mini Kit (Qiagen) according to manufacturer instructions. Barcoded libraries were prepared using the SmartSeq2 protocol as previously described³³ using a Hamilton NGS-STAR library preparation automation system at the BI Sequencing Facility and sequenced using a HiSeq 2500 (Illumina).

RNA-seq reads were trimmed using Trim Galore v.0.4.4 using default parameters to remove the Nextera adaptor sequence. Mapping was performed using HISAT2 v.2.1.0 against the mouse NCBIM37 genome, guided by gene models from Ensembl annotation release 68. Aligned fragments were imported into SeqMonk (v.1.44.0) and filtered to remove mappings with MAPQ scores of <20. Differential gene expression analysis was performed using the DESeq2 algorithm within SeqMonk.

Analysis of STAT5 binding

Naive CD4 $^+$ CD62L $^+$ CD44 $^-$ cells were sorted by FACS and stimulated on anti-CD3-coated plates in the presence of recombinant human IL-2 (5 ng ml $^{-1}$), TGF- β (2 ng ml $^{-1}$) and anti-CD28 (2 μ g ml $^{-1}$) for 4 days. Cells were washed thrice in complete medium and rested overnight in complete medium without IL-2. The following day, cells were stimulated with or without 50 ng ml $^{-1}$ IL-2 for 1 h and immediately chemically cross-linked using methanol-free formaldehyde (1% final w/v) at 37 °C for 10 min and the reaction was quenched with glycine. Ten million cells per ChIP replicate were sonicated to generate fragmented chromatin which was subjected to immunoprecipitation using anti-STAT5B (R&D AF1584) to detect STAT5 binding. For PCR-based confirmation of STAT5 binding, quantitative PCR reactions were carried out on input and immunoprecipitated DNA using the Power SYBR Green kit (Applied Biosystems) and the following primers: *Lrrc32+70k_FW1*, GAGCTGGGTG GTGGATAACA; *Lrrc32+70k_RV1*, CCAAGAAAA GGCGGGTGT; *Foxp3_CNS2_FW1*, ATCTGGCCA AGTCAGGT TGTGAC; *Foxp3_CNS2_RV1*, GGGCGTTCC TGTTTGACT GTTTCT; *Lrrc32_pro_FW1*, CCTTCTCCCT CCAGTCGTT; *Lrrc32_pro_RV1*, CGCCCCCCTT TTAAATAGC.

Analysis of genome-wide chromatin accessibility using ATAC-seq

Genome-wide measurement of chromatin accessibility and computational alignment of generated data were performed from biological replicates using ATAC-seq on FACS-sorted CD4 $^+$ *Foxp3* $^{eGFP+}$ T_{reg} and CD4 $^+$ *Foxp3* $^{eGFP-}$ T_{conv} cells from *Foxp3* eGFP reporter mice as previously described³⁴. ATAC-seq reads were trimmed using Trim Galore (v.0.4.4) using default parameters to remove standard Illumina adaptor sequences. Reads were mapped to the mouse NCBIM37 genome assembly using Bowtie2 v.2.3.2 with default parameters. TDF files for analysis in the IGV genome browser were generated using Samtools v.1.9 and Igvtools v.2.3.26 and differential accessibility of called peaks (MACS) was assessed using Diffbind.

Analysis of serum cytokines

Blood was collected into microcentrifuge tubes without anti-coagulants and centrifuged at 400g for 5 min. Supernatants were collected into fresh tubes and centrifuged at 16,000g for 10 min and stored at -80 °C until further analysis. Serum was analysed using the MesoScale Discovery Mouse proinflammatory cytokine bead array (MSD; K15048D-2) at the Core Biochemical Assay Laboratory at the University of Cambridge.

Syntenic alignment

Synteny data and alignment blocks were obtained from human:mouse LASTz alignments extracted from Ensembl compara database v.90. Chromosomal synteny was also taken from compara and LASTz pairwise alignments. The search is run in two steps: first, we searched for alignment blocks that were in the same order in the two genomes. Syntenic alignments that were closer than 200 kb were grouped into a synteny block; second, groups that were in synteny were linked, provided that no more than two non-syntenic groups were found between them and they were less than 3 Mb apart. For analysis of evolutionarily conserved transcription factor binding sites, we used the phyloP evolutionary conservation analysis providing basewise conservation among 30 placental mammals (phyloP30wayPlacental) to determine the level of evolutionary conservation at specified regulatory elements within the

enhancer³⁵. Evolutionarily conserved predicted transcription factor binding motifs were identified using ECR Browser (<https://ecrbrowser.org/>).

Human T_{reg} cell hQTL and eQTL analysis

Leukocyte cones were obtained with informed consent with Research Ethics Committee approval from donors at NHS Blood and Transplant, Cambridge (REC 15/NW/0282) and from the NHS Blood and Transplant, Oxford (REC 15/NS/0060) and experiments involving human samples complied with all relevant ethical regulations. T_{reg} cells from 135 healthy adults of Caucasian origin were obtained from leukodepletion cones. Peripheral blood mononuclear cells (PBMCs) were isolated using Lympholyte-H (Cedarlane Labs) density gradient centrifugation. The CD4⁺ T cell fraction of the PBMCs was obtained by negative selection using EasySep Human CD4⁺ T Cell Enrichment Kit (StemCell Technologies, 19052) following the manufacturer's instructions. CD4⁺CD127⁻CD25⁺ T_{reg} cells were isolated by FACS. Genomic DNA was extracted from each sample and subjected to genotyping using the Infinium CoreExome-24 v.1.1 BeadChip (Illumina). The genotyping data were imputed using the 1000 Genomes Phase 3 reference panel and BEAGLE 4.1³⁶. T_{reg} cells obtained from each individual were analysed by RNA-seq (123 individuals) or genome-wide measurement of H3K27ac using ChIPmentation-seq (91 individuals)³⁷. A total of 1.86 million read pairs were downsampled from each donor per H3K27ac ChIPmentation-seq assay and merged. Then, H3K27ac broad peaks were called using MACS2³⁸ and only peaks with fold enrichment ≥ 2 and adjusted *P* value <0.001 were maintained in the final set. Gene and peak read counts were obtained using featureCounts³⁹. Quantitative trait loci (QTL) for gene expression and H3K27ac were evaluated using linear models with QTLtools⁴⁰. Principal components that explained up to 1% of the observed variance per assay were included as covariates. Colocalization between QTLs and immune disease genome-wide association study (GWAS) loci was performed using coloc v.2.3⁴¹ and using a 400-kb window around each lead QTL variant located within 100 kb from each GWAS variant (nominal *P* value $<10^{-5}$), as described⁴².

For eQTL analysis of signal-driven GARP expression on T_{reg} cells, PBMCs were collected from presumed healthy donors at the Policlinico San Matteo Pavia Fondazione IRCCS and 1×10^7 cells per donor were cryopreserved for later analysis. Following cryorecovery, cells were stimulated at 37 °C, 5% CO₂ for 16 h in RPMI culture medium supplemented with 10% fetal calf serum (Sigma), 1% pen/strep (Gibco) and 50 µM β-mercaptoethanol, non-essential amino acids (Gibco) and Glutamax (Gibco). Cells were plated at a density of 1×10^6 cells per well on 24-well plates in the presence or absence of 50 ng ml⁻¹ recombinant human IL-2 (Peprotech) and plate-bound anti-CD3 (0.2 µg ml⁻¹; clone OKT3 BioXcell BE0001-2) and anti-CD28 (0.2 µg ml⁻¹; clone 9.3 BioXcell BE0248) monoclonal antibodies. For genotyping of individuals, genomic DNA extracted from PBMCs was subjected to PCR-based amplification using the following primers: Fw1: 5'-AAAGCATGGCTGAGAAAAC-3' and Rv1: 5'-CCAGGGAGGAAGTTCTGGAG-3' yielding an amplicon containing rs11236797 and forward and reverse Sanger sequencing reactions were primed using Fw1 and Rv2 (5'-ACAGTGCTGACTGAGAGGAA-3', respectively.

HiChIP v4C analysis

v4C analyses were performed using matrices generated by Juicebox. The Juicebox tools dump command was used to extract the chromosome of interest from the .hic file²⁹. The interaction profile of the specific 5-kb bins containing the promoter and enhancer anchors were then plotted in R. Replicate reproducibility was visualized with the mean profile shown as a line and the shading surrounding the mean representing the standard deviation between replicates. The *P* value was calculated using Student's *t* test comparing the replicate read support for the promoter to enhancer interaction in T_{reg} cells versus naive T cells.

Lentiviral plasmid construction and virus production

Lenti sgRNA(MS2)_zeo (plasmid 61427; Addgene), dCas9-VP64_GFP (plasmid 61422; Addgene) and Lenti MS2-P65-HSF1_Hygro (plasmid 61426; Addgene)⁴³ vectors were gifts from F. Zhang. DNA sequences of single guide RNAs (sgRNAs) for CRISPR activation were designed using Custom Alt-R CRISPR-Cas9 guide RNA design tool (https://www.idtdna.com/site/order/designtool/index/CRISPR_CUSTOM) and are listed in Supplementary Table 6. All sequences were selected to precede a NGG protospacer-adjacent motif sequence. Cloning of sgRNAs into lenti sgRNA(MS2)_zeo was performed as previously described⁴⁴. For the production of lentiviruses pseudotyped with the vesicular stomatitis virus G protein envelope, plasmid DNA was co-transfected with vesicular stomatitis virus G protein, pLP1, and pLP2 plasmids into HEK293T cells (ATCC; mycoplasma-free low passage stock) using Lipofectamine 3000 (Invitrogen) according to the manufacturer's protocol and as previously described⁴⁴.

PBMCs were obtained from healthy individuals at New York Blood Center with NYBC Institutional Review Board approval and experiments complied with all relevant ethical regulations. Lymphocytes were isolated using Ficoll-Paque plus (GE Healthcare). CD4⁺ T cells were isolated using Dynal CD4⁺ isolation kits (Invitrogen). Purified CD4⁺ T cells were stimulated using anti-CD3/anti-CD28 Dynabeads (Invitrogen) and cultured in complete RPMI 1640 medium (RPMI1640 supplemented with 10% FBS; Atlanta Biologicals) containing IL-2 (10 ng ml⁻¹) as described⁴⁴. One day after activation, cells were transduced with dCas9-VP64_GFP and Lenti_MS2-P65-HSF1_Hygro lentiviral vectors at multiplicity of infection (MOI) of 5–10. Cells were then selected with 250 µg ml⁻¹ hygromycin 3–5 days post-infection and expanded for 2 weeks. Antibiotic selection was performed for 3–5 days or until 95% of non-transduced cells were dead. Expanded and hygromycin-selected T cells expressing dCas9-VP64-GFP and P65 were then re-stimulated with anti-CD3-anti-CD28 beads and transduced with lentiviruses encoding Enhancer-targeting sgRNAs in lenti-sgRNA_(MS2) at a MOI of 5–10. Cells were collected 5 days after transduction and analysed by flow cytometry on a SP6800 spectral cell analyser (Sony Biotechnology). Data analysis was performed using FlowJo software (TreeStar).

Statistical analysis

Where relevant, sample sizes were determined using power calculations on the basis of variability observed in prior experiments of a similar kind or using prior experience of sample size requirement. For experiments where technical limitations prevented adequate statistical power to be obtained from single experiments, results from multiple experiments were pooled to provide sufficient statistical power. Pre-established exclusion criteria across samples from a given experiment were used to avoid subjective bias. Experiments included positive and negative controls to allow technical failure of experiments to be objectively determined. Data reported are in most cases non-subjective and did not require randomization or blinding at measurement. However, where appropriate, experimental cohorts were composed of randomized age- and sex-matched mice or subject to random Mendelian segregation of genotypes within litters. Investigators were not formally blinded. However, in randomized experiments it was difficult for investigators and technicians to readily determine genotypes from animal identifiers at the bench.

Reporting summary

Further information on research design is available in the Nature Research Reporting Summary linked to this paper.

Data availability

RNA-seq data have been deposited in the Gene Expression Omnibus (GEO) database under the accession number GSE128198.

Article

Sequencing data for H3K27ac hQTL and mRNA eQTL analyses are deposited under the European Genome-phenome Archive (EGA; study accession EGAS00001003516, datasets EGAD00001004828 and EGAD00001004830).

31. De Cuyper, I. M. et al. A novel flow cytometry-based platelet aggregation assay. *Blood* **121**, e70–e80 (2013).
32. Asseman, C., Mauze, S., Leach, M. W., Coffman, R. L. & Powrie, F. An essential role for interleukin 10 in the function of regulatory T cells that inhibit intestinal inflammation. *J. Exp. Med.* **190**, 995–1004 (1999).
33. Picelli, S. et al. Full-length RNA-seq from single cells using Smart-seq2. *Nat. Protoc.* **9**, 171–181 (2014).
34. Buenrostro, J. D., Giresi, P. G., Zaba, L. C., Chang, H. Y. & Greenleaf, W. J. Transposition of native chromatin for fast and sensitive epigenomic profiling of open chromatin, DNA-binding proteins and nucleosome position. *Nat. Methods* **10**, 1213–1218 (2013).
35. Pollard, K. S., Hubisz, M. J., Rosenbloom, K. R. & Siepel, A. Detection of nonneutral substitution rates on mammalian phylogenies. *Genome Res.* **20**, 110–121 (2010).
36. Browning, B. L., Zhou, Y. & Browning, S. R. A one-penny imputed genome from next-generation reference panels. *Am. J. Hum. Genet.* **103**, 338–348 (2018).
37. Schmidl, C., Rendeiro, A. F., Sheffield, N. C. & Bock, C. ChIPmentation: fast, robust, low-input ChIP-seq for histones and transcription factors. *Nat. Methods* **12**, 963–965 (2015).
38. Zhang, Y. et al. Model-based analysis of ChIP-Seq (MACS). *Genome Biol.* **9**, R137 (2008).
39. Liao, Y., Smyth, G. K. & Shi, W. featureCounts: an efficient general purpose program for assigning sequence reads to genomic features. *Bioinformatics* **30**, 923–930 (2014).
40. Delaneau, O. et al. A complete tool set for molecular QTL discovery and analysis. *Nat. Commun.* **8**, 15452 (2017).
41. Giambartolomei, C. et al. Bayesian test for colocalisation between pairs of genetic association studies using summary statistics. *PLoS Genet.* **10**, e1004383 (2014).
42. Bossini-Castillo, L. et al. Immune disease variants modulate gene expression in regulatory CD4+ T cells and inform drug targets. Preprint at *bioRxiv* <https://doi.org/10.1101/654632> (2019).
43. Perez-Pinera, P. et al. RNA-guided gene activation by CRISPR–Cas9-based transcription factors. *Nat. Methods* **10**, 973–976 (2013).
44. Chen, X. et al. Functional interrogation of primary human T cells via CRISPR genetic editing. *J. Immunol.* **201**, 1586–1598 (2018).
45. Demenais, F. et al. Multiancestry association study identifies new asthma risk loci that colocalize with immune-cell enhancer marks. *Nat. Genet.* **50**, 42–53 (2018).

Acknowledgements The research was supported by Wellcome Trust–Royal Society Fellowship 105663/Z/14/Z, Wellcome Trust grant WT206194, Biotechnology and Biological Sciences Research Council grants BB/N007794/1, BBS/E/B/000C0427 and BBS/E/B/000C0428, Cancer Research UK grant C52623/A22597, Medical Research Council grants MR/N014995/1, MR/S024468/1 and MC_UU_00014/5, Wellcome Trust Major Award 208363/Z/17/Z, Associazione Italiana per la Ricerca sul Cancro (AIRC) grant IG 20607, and US National Institutes of Health (NIH) grants RM1-HG007735, U19-AI142733 and R01-AI121920. We thank members of the Babraham Institute Biological Services Unit, flow cytometry facility and sequencing facility, and Wellcome Sanger Institute flow cytometry, sequencing, IT and data access facilities for data generation and processing. We thank all participating blood donors, and Cambridge and Oxford NHS Blood and Transplant, New York Blood Center and Policlinico San Matteo Pavia Fondazione for the recruitment of study participants. We thank F. De Paoli (Humanitas) for processing human PBMC samples and M. Turner, K. Okkenhaug, E. Shevach, M. Linterman and G. Butcher for support and discussion.

Author contributions R.N., C.J.I., F.M.G., M.D., L.P., L.K., P.K., F.S., S.K.W., A.C., P.V., C.E.W., T.L., T.F., H.F., E.L., D.U., S.M. and R.R. performed experiments. L.B.-C., D.G. and G.T. performed and analysed hQTL and eQTL analyses of human T cells. R.N., C.J.I., F.S., M.R.M., H.F., J.V., A.L., S.A., G.T. and R.R. analysed data. R.N., C.J.I., L.B.-C., G.T. and R.R. wrote the manuscript. H.Y.C., D.U., G.T. and R.R. provided overall supervision of the work.

Competing interests The authors declare no competing interests.

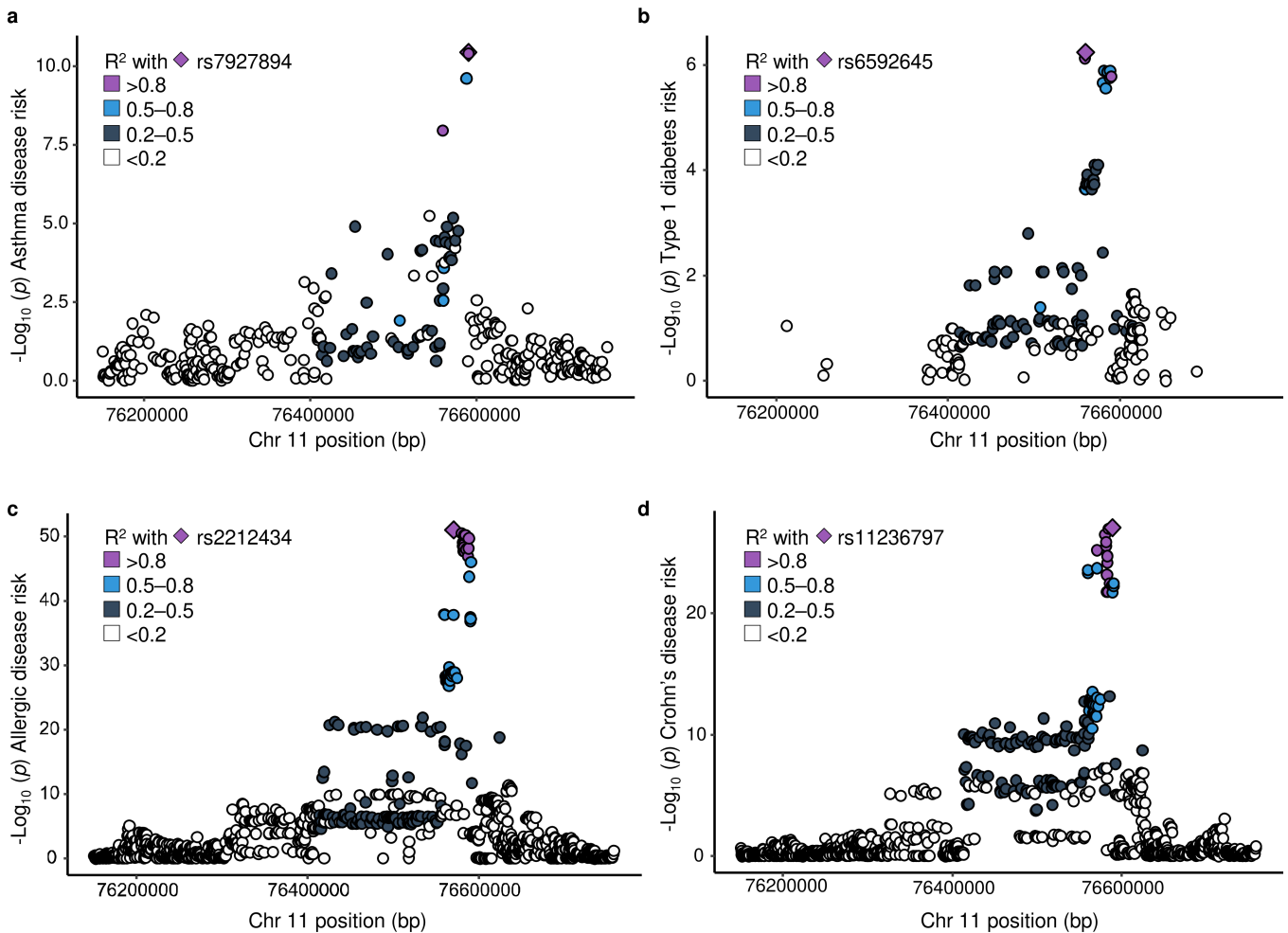
Additional information

Supplementary information is available for this paper at <https://doi.org/10.1038/s41586-020-2296-7>.

Correspondence and requests for materials should be addressed to C.J.I., G.T. or R.R.

Peer review information *Nature* thanks Arthur Kaser, Shimon Sakaguchi and the other, anonymous, reviewer(s) for their contribution to the peer review of this work.

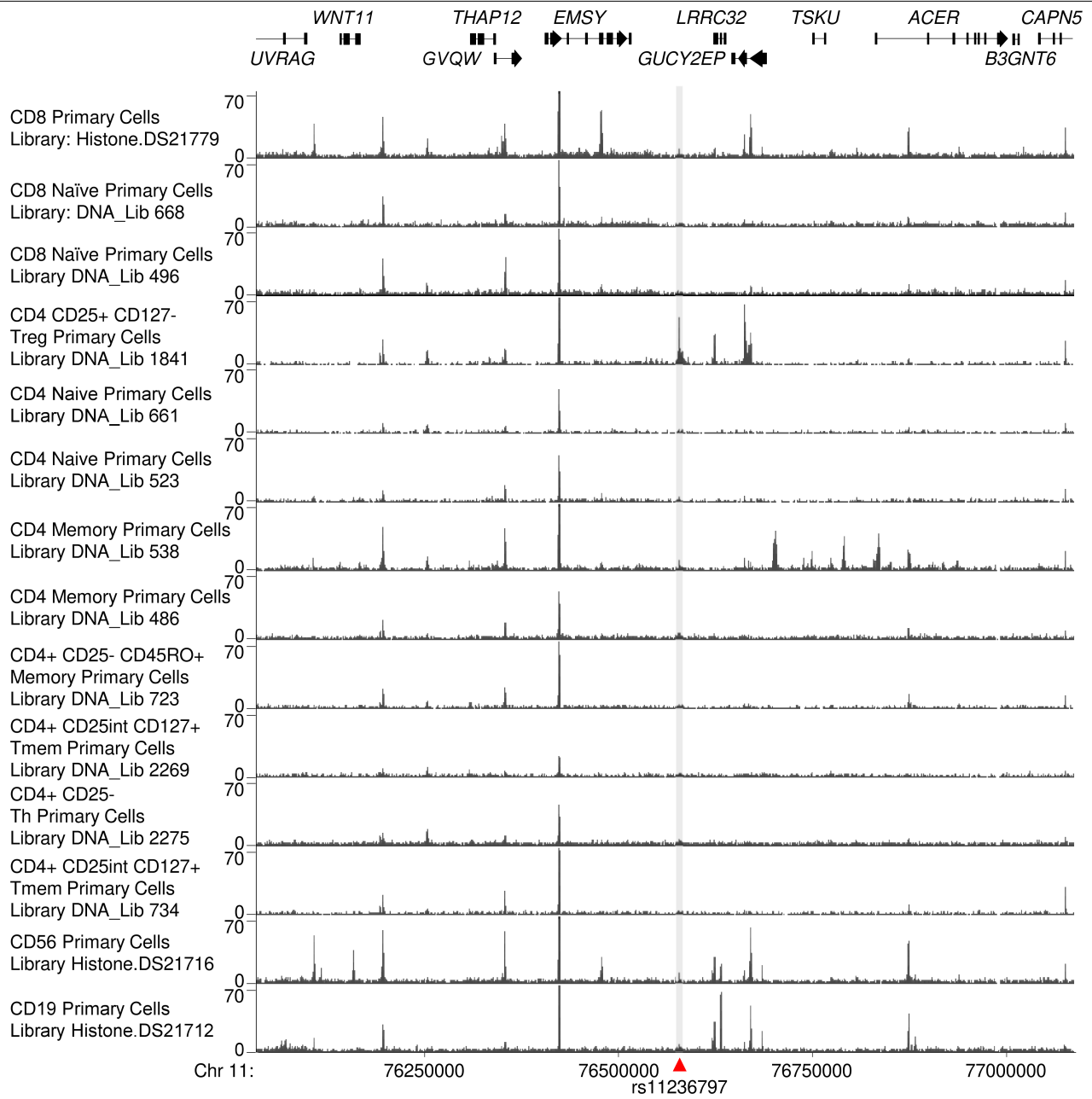
Reprints and permissions information is available at <http://www.nature.com/reprints>.



Extended Data Fig. 1 | Highly linked genetic polymorphisms at a distal intergenic region of 11q13.5 are associated with risk of multiple immune-mediated diseases. **a–d.** Graph showing association of polymorphisms within the 11q13.5 locus with risk of indicated immune-mediated disorders ($-\log_{10}(P)$; left axis). Each point represents an

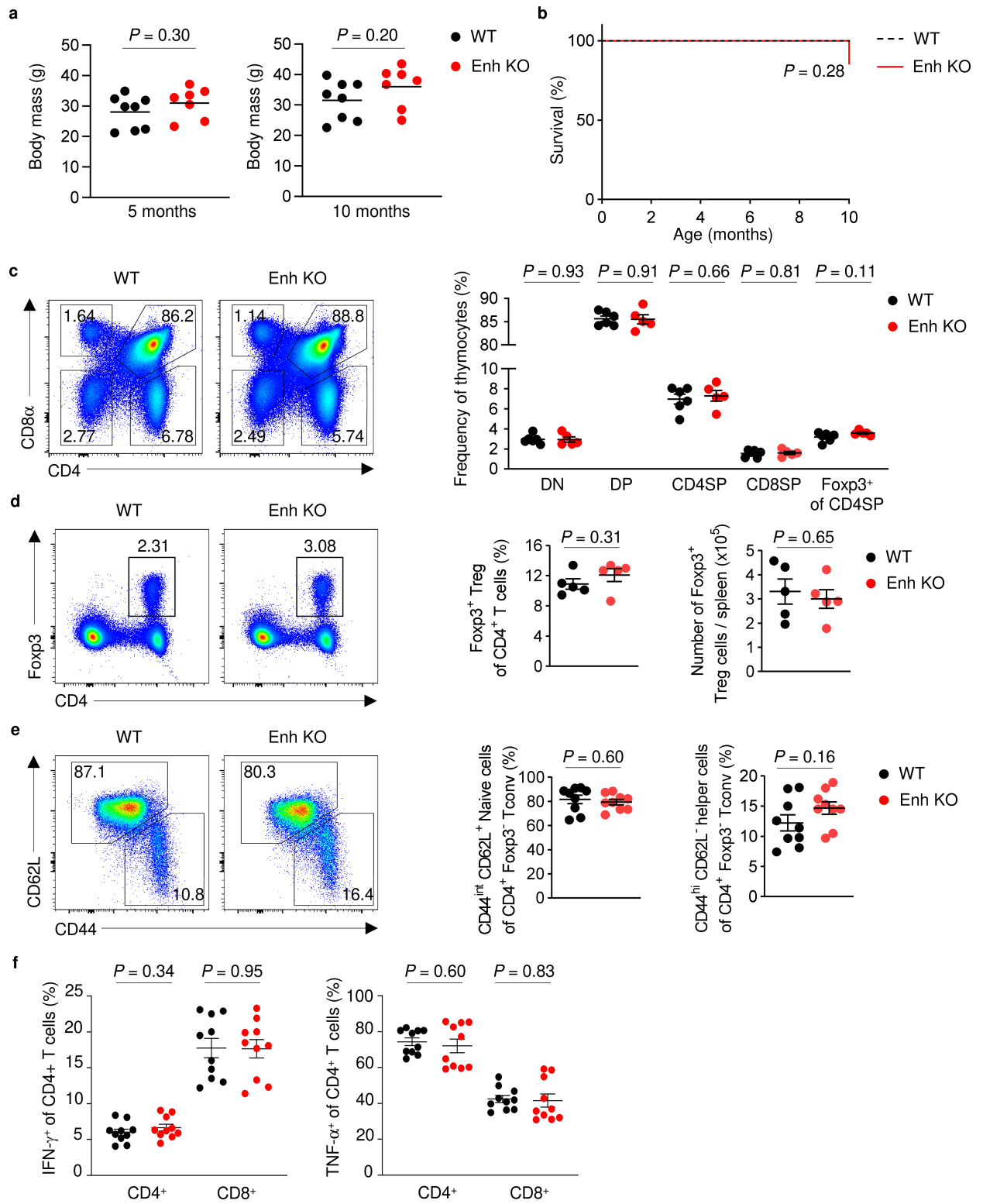
individual SNP. Point colours depict R^2 values reflecting the level of linkage disequilibrium between each polymorphism and the indicated lead GWAS variant (diamond symbol). Chromosomal position (GRCh38) is represented on the x-axis. GWAS summary statistics and replicate information from ref.⁴⁵ (a), ref.⁴ (b) ref.⁶ (c) and ref.² (d).

Article



Extended Data Fig. 2 | Alignments showing distribution of H3K27ac at the indicated genomic region in primary human lymphocytes. Alignment of H3K27ac enrichment at the indicated locus within the indicated lymphocyte lineages; sample information and replicate statistics are from the Roadmap

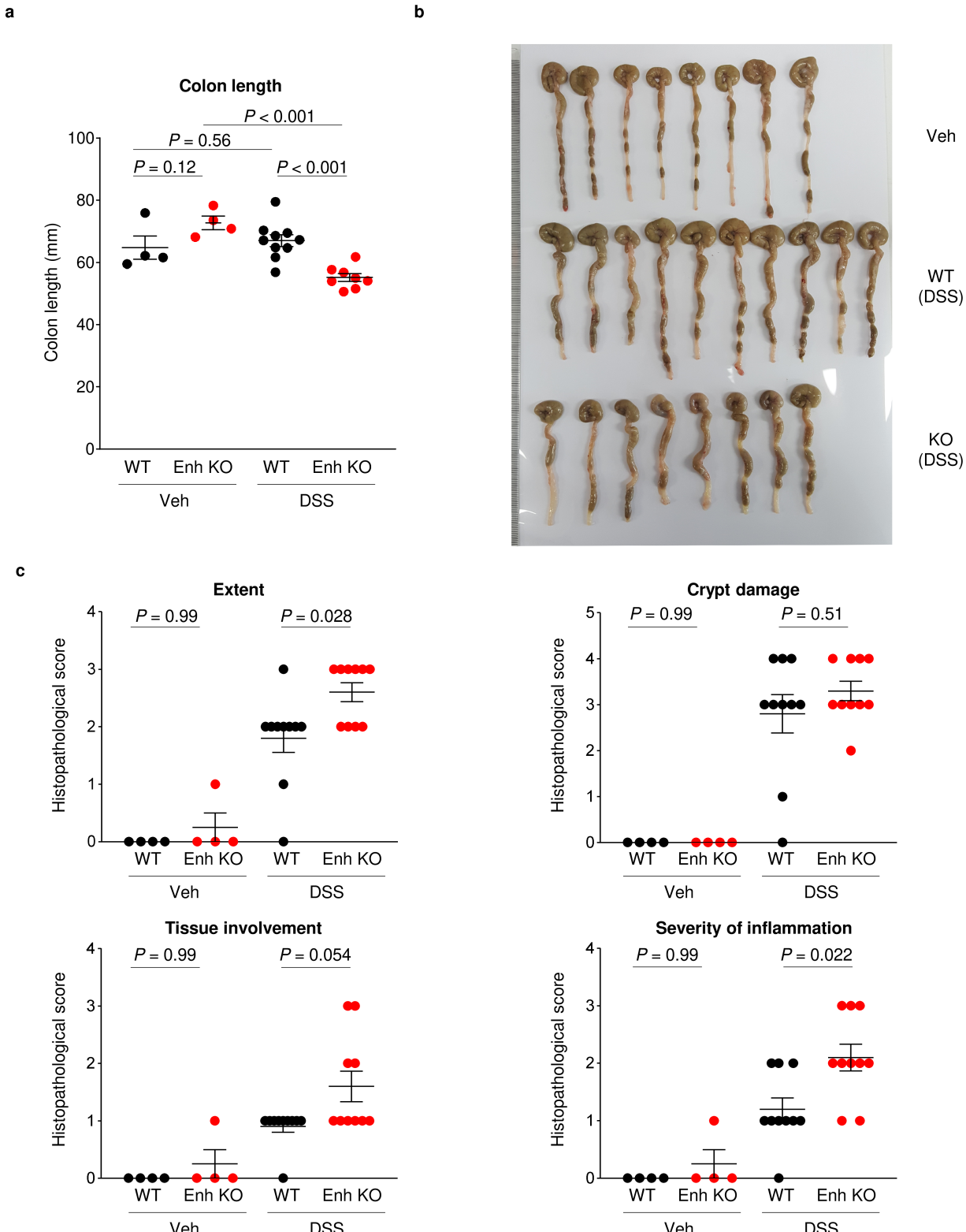
Epigenomics Project⁸. Grey shaded area marks the risk locus containing the single nucleotide polymorphism (SNP) rs11236797 (position indicated by red triangle).



Extended Data Fig. 3 | Steady-state immune phenotype of Enh-KO mice.

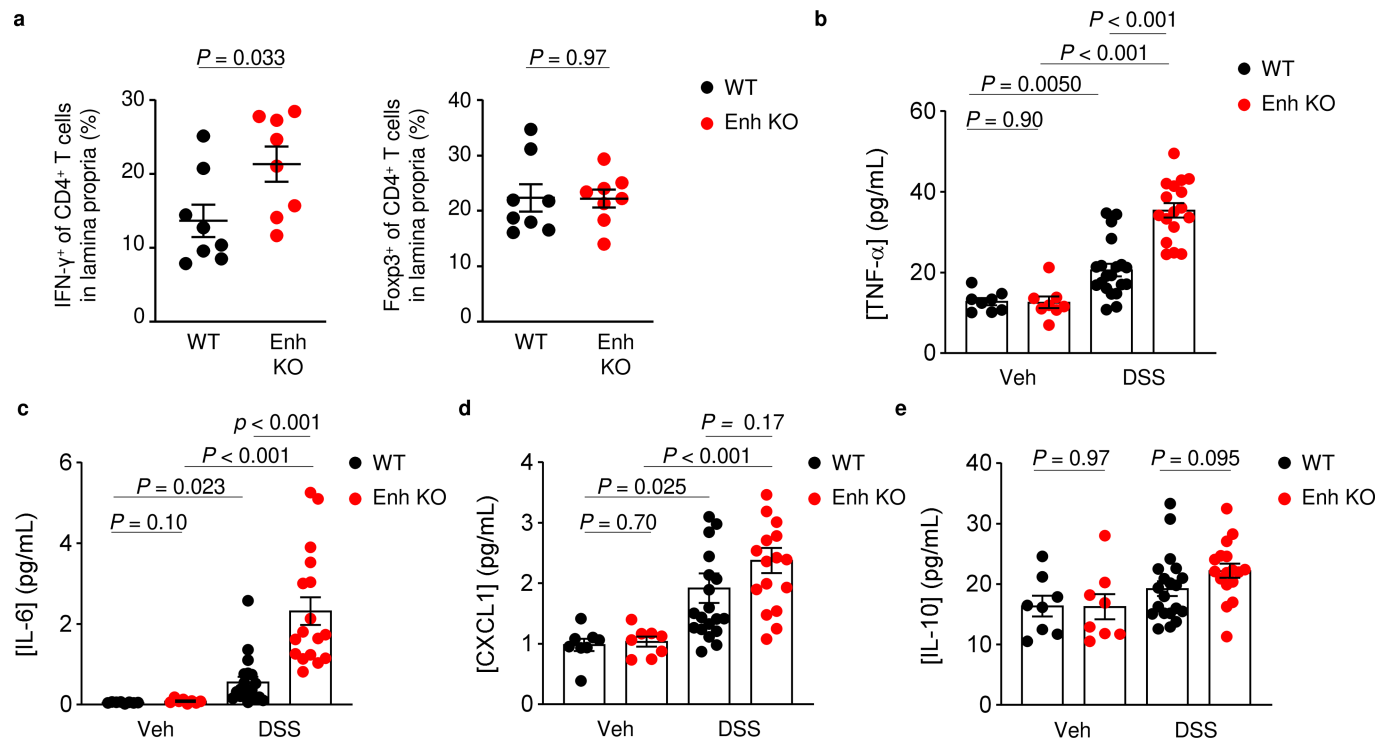
a, b, Body mass at indicated age (**a**) and Kaplan–Meier plot showing survival (**b**) of mice of indicated genotypes ($n=8$ and 7 , WT and Enh-KO from 8 independent breedings). **c**, Representative flow cytometry (left) and replicate measurements (right) of the frequency of the indicated thymocyte subsets in the thymi of mice of the indicated genotypes at $8\text{--}10$ weeks of age ($n=6$ and 5 ; WT and Enh-KO). **d**, Representative flow cytometry (left) and replicate measurements of the frequency and absolute number (right) of Foxp3 $^{+}$ T $_{reg}$ cells in the spleens of mice of the indicated genotypes at $8\text{--}10$ weeks of age ($n=5$ mice per group). Representative of two independent experiments (**c, d**).

e, Representative flow cytometry (left) and replicate measurements of the frequency of naive and helper CD4 $^{+}$ Foxp3 $^{-}$ T $_{conv}$ cells in the spleens of mice of the indicated genotypes at $8\text{--}10$ weeks of age ($n=9$ mice per group, pooled from two independent experiments). **f**, Frequency of cells expressing IFN- γ (left) and TNF (right) upon intracellular cytokine staining analysis of splenic CD4 $^{+}$ and CD8 $^{+}$ T cells from mice of the indicated genotypes at $8\text{--}10$ weeks of age ($n=10$ mice per group pooled from two independent experiments). Unpaired two-tailed Student's t test (**a, c-f**), Mantel–Cox test (**b**). Data are mean \pm s.e.m.



Extended Data Fig. 4 | Increased susceptibility of Enh-KO mice to colitis induced by DSS. **a, b**, Replicate length measurements (a) and photographs (b) of large intestine from WT and Enh-KO mice treated with DSS or vehicle control (vehicle). $n=4$ (WT vehicle), 4 (Enh-KO vehicle), 10 (WT DSS) and 8 (Enh-KO DSS). **c**, Histopathological scores of sections of large intestine from WT and Enh-KO treated for 16 days with DSS or vehicle. The following scoring criteria were used: extent of inflammation: 0, none; 1, mucosa; 2, mucosa and

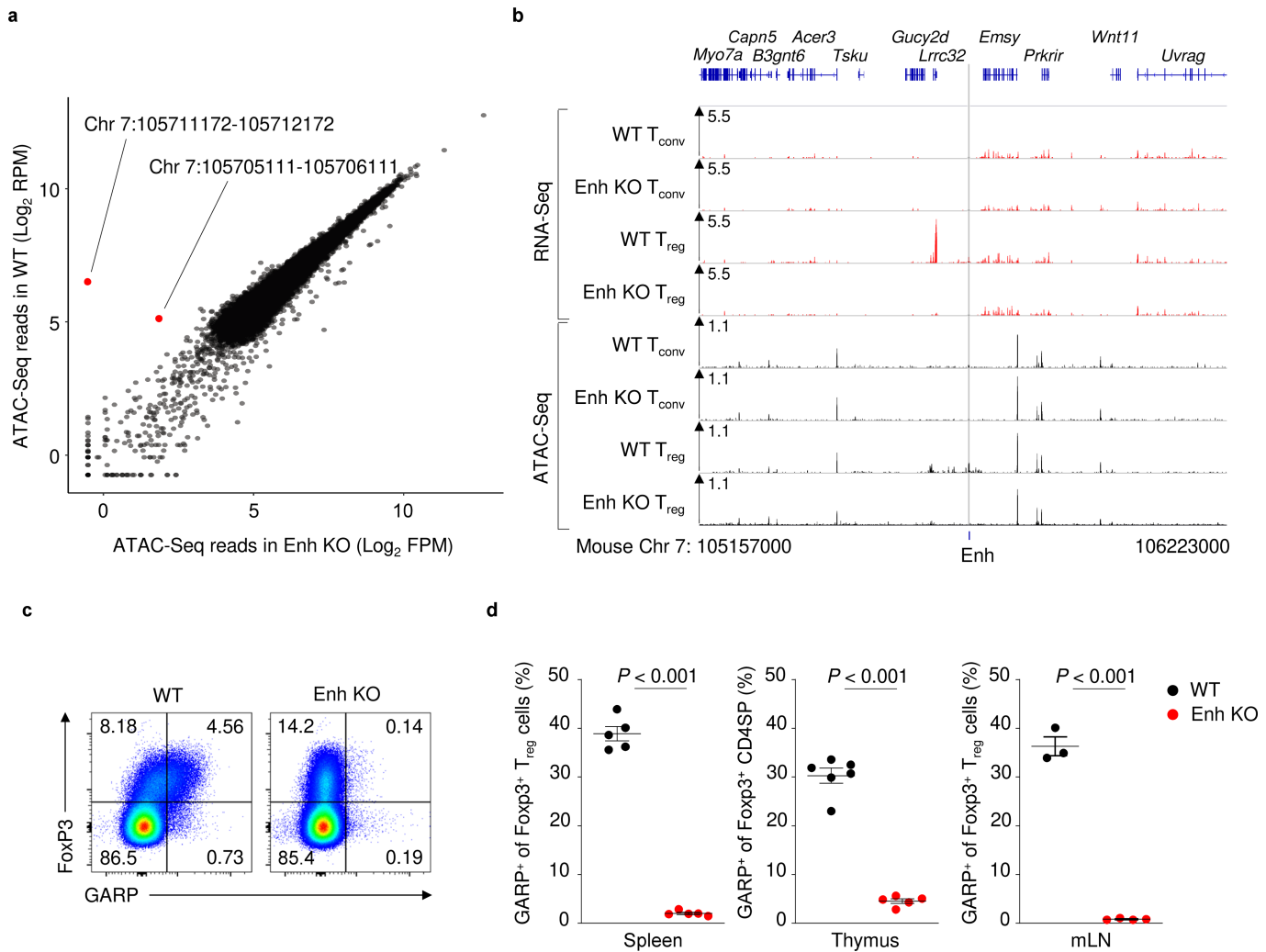
submucosa; 3, transmural. Crypt damage: 0, none; 1, basal one-thirds; 2, basal two-thirds; 3, only surface epithelium intact; 4, loss of entire crypt and surface epithelium. Tissue involvement: 1, 0 to 25%; 2, 26 to 50%; 3, 51 to 75%; 4, 76 to 100%. Severity of inflammation: 0, none; 1, mild; 2, moderate; 3, severe. Data are representative of two independently repeated experiments with 10 and 4 mice per DSS- and vehicle-treated group. Unpaired two-tailed Student's *t* test (a); Wilcoxon-Mann-Whitney Test (c). Data are mean \pm s.e.m.



Extended Data Fig. 5 | Analysis of cytokine expression in WT and Enh-KO mice treated with DSS. **a**, Replicate measurements of IFN- γ (left) and Foxp3 (right) in CD4 $^+$ T cells from large intestinal lamina propria ($n=8$ mice per group). Data representative of two independent experiments.

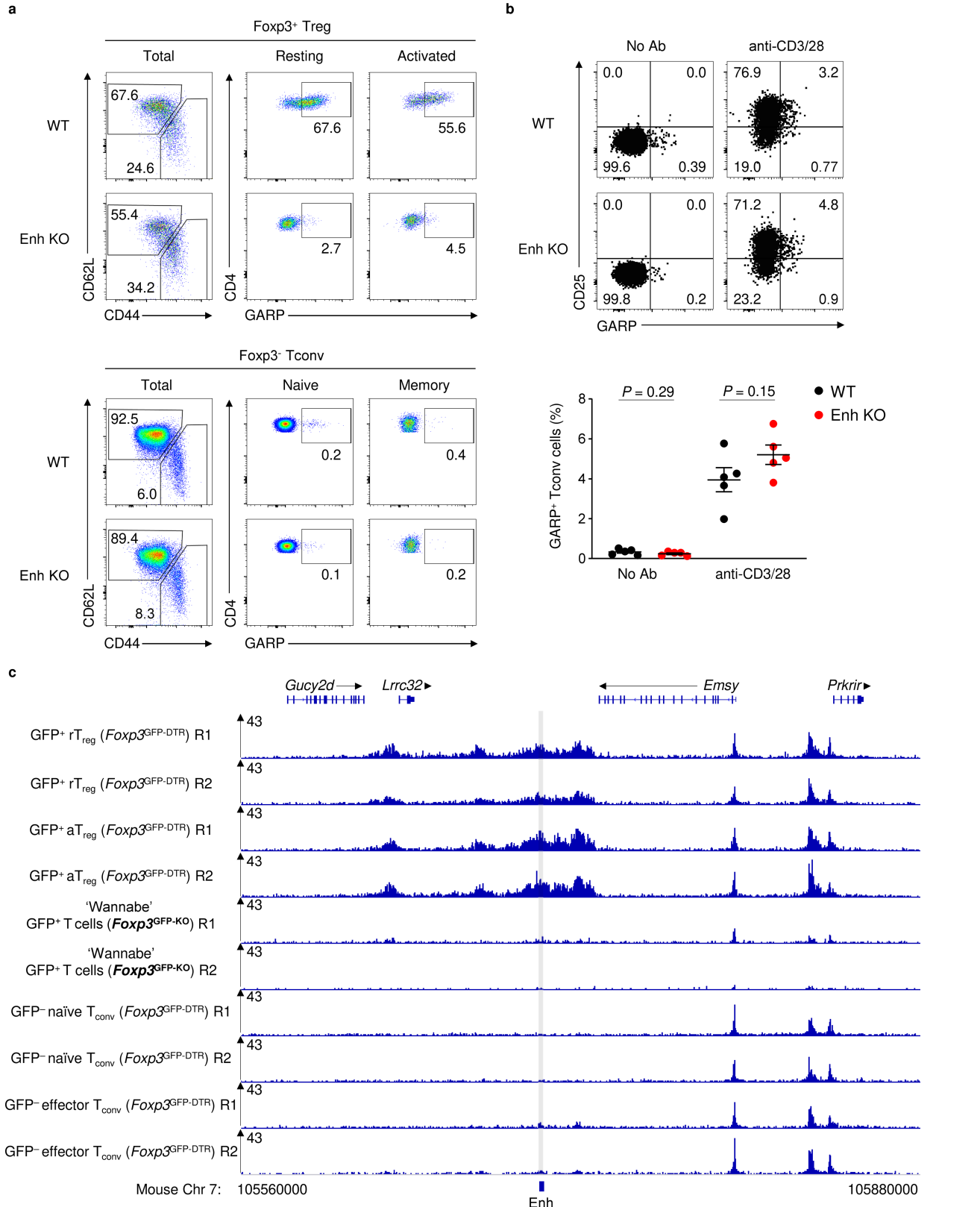
b–e, Concentration of the indicated cytokines in the serum of WT and Enh-KO

mice treated with vehicle or DSS for 16 days. Data pooled from two independent experiments with $n=8, 8, 20$ and 17 for WT (vehicle), Enh-KO (vehicle), WT (DSS), Enh-KO (DSS) groups. Data analysed using unpaired two-tailed Student's t test. Data are mean \pm s.e.m.



Extended Data Fig. 6 | Loss of Lrrc32 and GARP expression in Foxp3⁺ T_{reg} cells from Enh-KO mice. **a**, Scatter plot showing global differences in chromatin accessibility at called peaks using ATAC-Seq analysis of WT and Enh-KO CD4⁺ Foxp3^{GFP+} T_{reg} cells. Red dots show significantly differentially accessible peaks (FDR < 0.05). Mean \log_2 reads per million (RPM) values for each called peak (represented as points) from three independent biological replicates are shown, with samples isolated on different days. Two-tailed Wald test with Benjamini–Hochberg correction. **b**, Representative alignment of gene expression (top) and chromatin accessibility (bottom) within the indicated cell types sorted by FACS from WT and Enh-KO Foxp3^{eGFP} reporter

mice. Expected loss of ATAC-seq reads mapping to the deleted region (Enh; highlighted in grey) in Enh-KO cells is observed. Data representative of three independent biological replicates with samples isolated on different days. **c**, Representative flow cytometry analysis of GARP and Foxp3 expression by CD4⁺ T cells of mice of the indicated genotypes from mesenteric lymph nodes. **d**, GARP expression from mice of indicated genotypes in spleen ($n=5$ per genotype), thymus ($n=6$ and 5 for WT and Enh-KO groups), and mesenteric lymph node ($n=3$ and 4 for WT and Enh-KO groups). Data are representative of three and two independent experiments (**c, d**). Unpaired two-tailed Student's t-test (**d**). Data are mean \pm s.e.m.



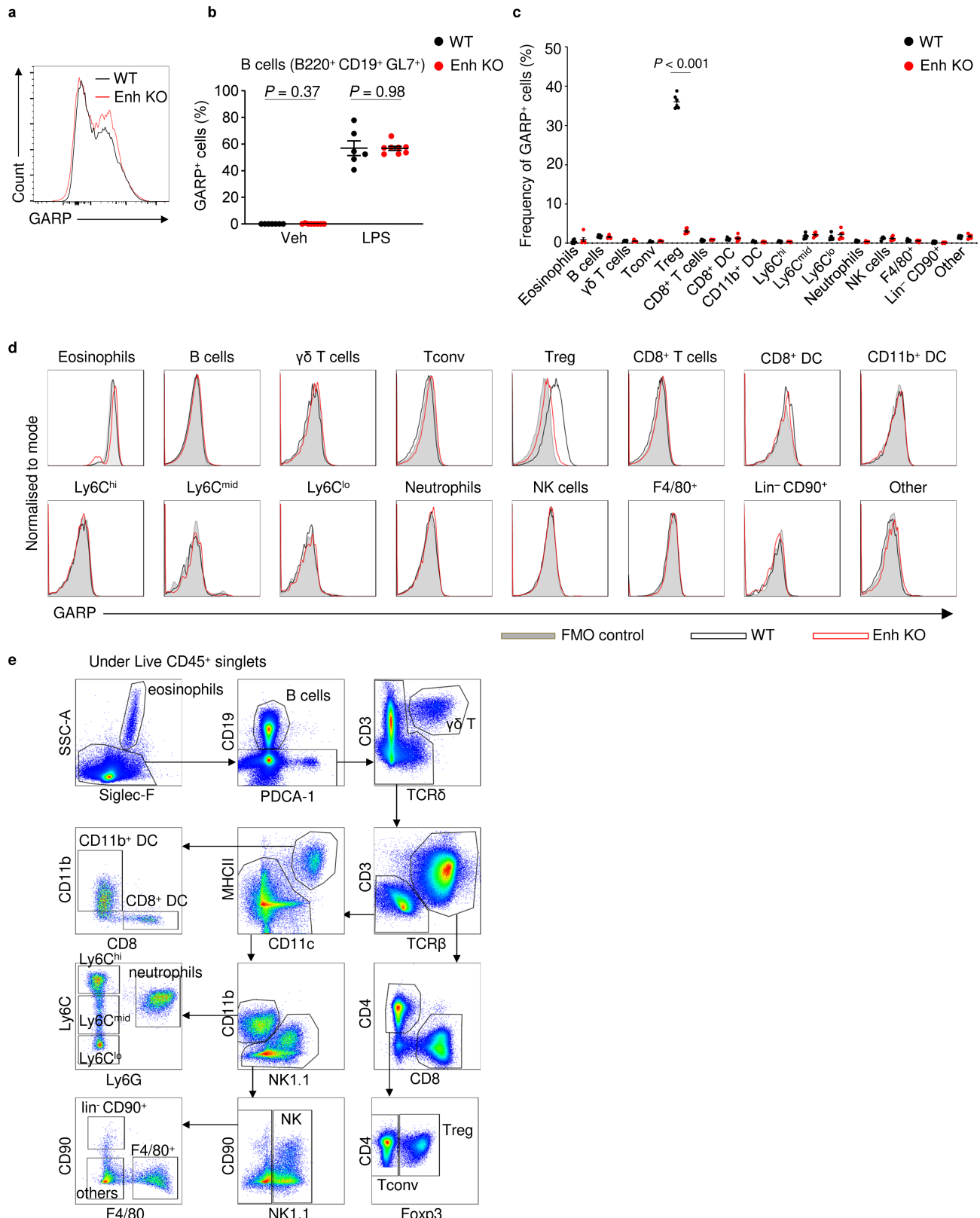
Extended Data Fig. 7 | *Lrrc32*+70k is not required for induction of GARP on the surface of CD4⁺T_{conv} cells following stimulation in vitro.

a, Representative flow cytometry showing gating strategy and representative GARP expression on resting (CD44^{low}CD62L⁺) and activated (CD44^{high}CD62L⁺) T_{reg} cells (top) and naive (CD44^{low}CD62L⁺) and memory (CD44^{high}CD62L⁺) T_{conv} cells (bottom). Data are representative of two independent experiments.

b, Representative flow cytometry (top) and replicate measurements (bottom)

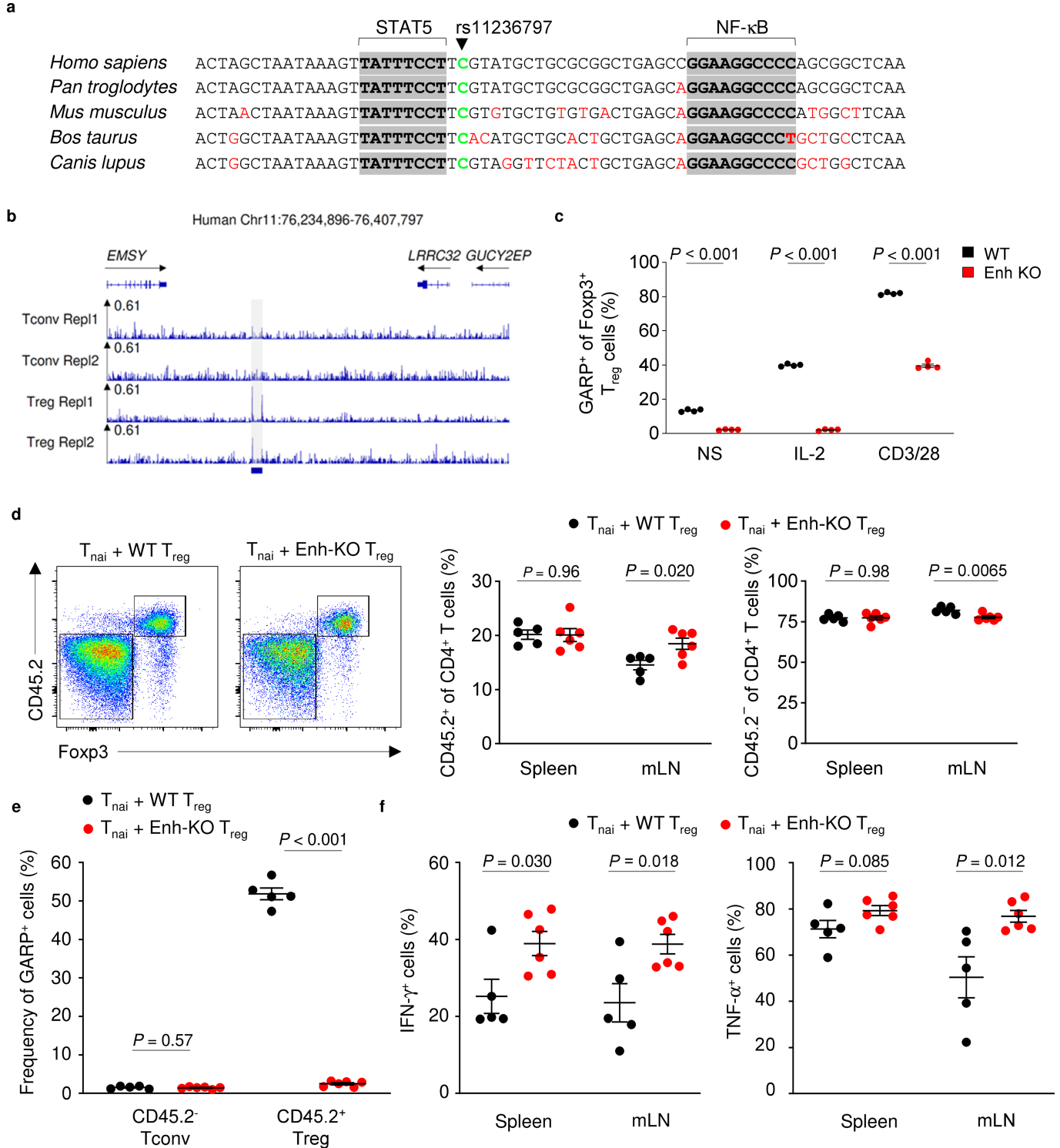
of CD25 and GARP expression in CD4⁺Foxp3⁻T_{conv} cells following stimulation under the indicated conditions for 16 h in vitro. Data representative of three independently repeated experiments with five independent biological replicates per group. **c**, Representative alignments of known H3K27ac ChIP-seq data from the indicated cell types. Sample information and replicate statistics are in ref.²⁰. Grey bar shows position of the enhancer. Unpaired two-tailed Student's *t* test (**b**). Data are mean ± s.e.m.

Article



Extended Data Fig. 8 | Specific loss of GARP expression on T_{reg} cells from Enh-KO mice. **a**, Representative flow cytometry of GARP expression on CD45⁻CD31⁺ endothelial cells from lungs of WT and Enh-KO mice. **b**, Frequency of GARP⁺ cells among WT and Enh-KO B220⁺CD19⁺GL7⁺ cells, stimulated with bacterial LPS or vehicle control (Veh) for 48 h ($n=6$ and 8 for WT and Enh-KO groups). **c**, Percentage of GARP⁺ cells among indicated cell types from WT and

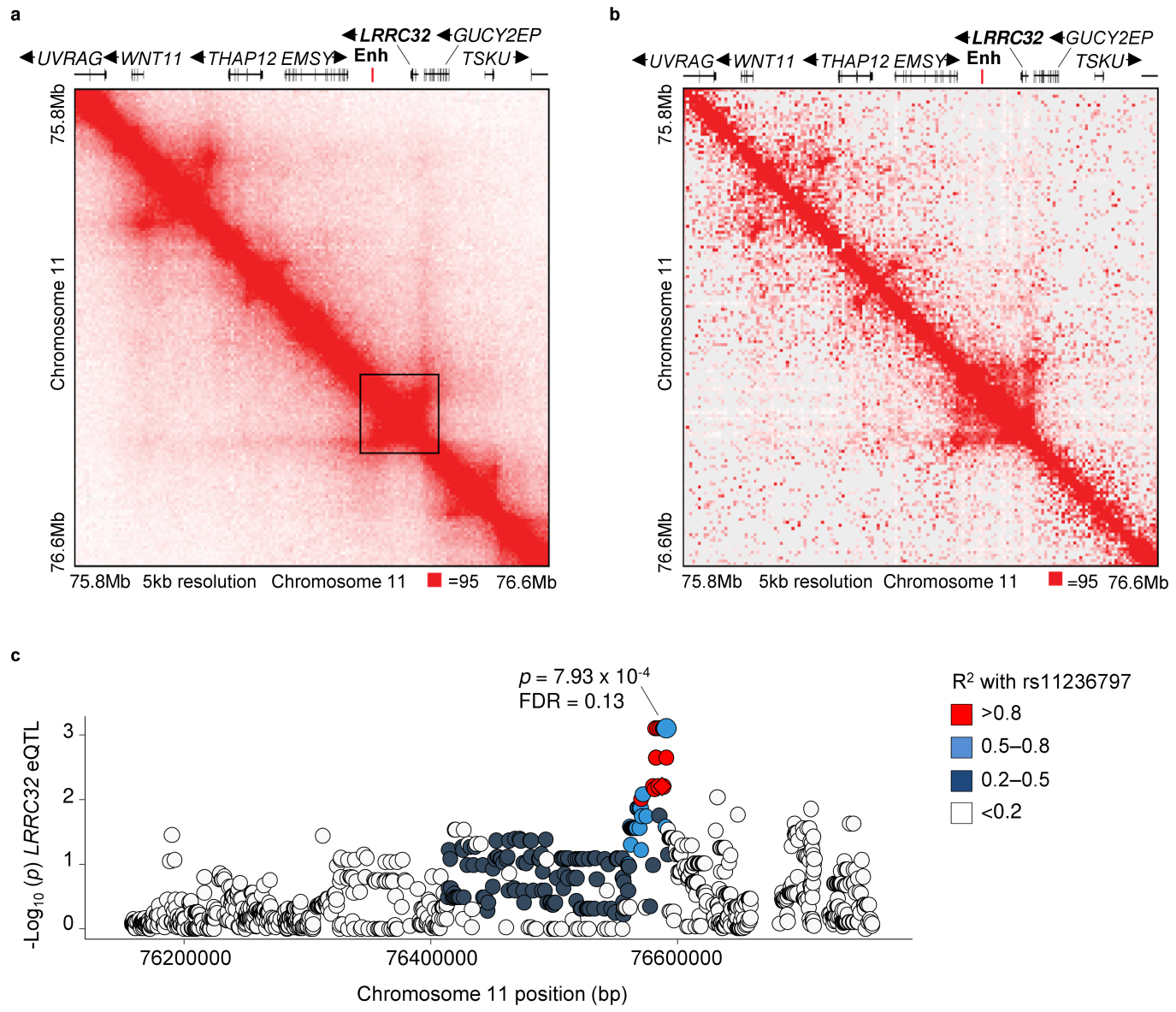
Enh-KO mice ($n=6$ per genotype; unpaired two-tailed Student's *t* test). **d**, Representative histograms showing GARP expression in the cell types shown in **c**. **e**, Representative flow cytometry indicating gating strategy for cells shown in **c**. Unpaired two-tailed Student's *t* test (**b**). Data are representative of two independent experiments. Data are mean \pm s.e.m.



Extended Data Fig. 9 | Molecular and functional characterization of mouse and human enhancer homologues. **a**, Evolutionarily conserved STAT5 and NF-κB binding motifs within *Lrrc32*+70k. Genomic sequence alignments of reference genome sequences of indicated mammals are shown. The position of conserved STAT5 and NF-κB binding motifs (V\$STAT5A_03 and V\$NFKAPPAB_01, respectively) are highlighted in grey. The position of rs11236797 is shown. **b**, Alignment of previously determined STAT5 ChIP-seq binding at the indicated locus in human T_{reg} and T_{conv} cells. Sample information and replicate statistics are in ref.²¹. The identified distal enhancer is shown indicated by the grey shaded area. **c**, GARP expression in CD4⁺Foxp3⁺ T_{reg} cells following stimulation under the indicated conditions for 16 h in vitro. $n = 4$ technical replicates per condition; data are representative of three independent experiments. **d**, Representative flow cytometry showing gating (left) and replicate measurements (right) of CD45.2⁺ (transferred T_{reg}) and CD45.2⁻ (transferred T_{conv}) cells within the spleen and mesenteric lymph node of cell-transfer recipients. **e**, Replicate measurements of GARP expression on the indicated cell types from the spleen. **f**, Replicate measurements of expression of indicated cytokines by CD45.2⁻ T_{conv} cells from indicated tissues following brief restimulation ex vivo. $n = 5$ and 6, WT and Enh-KO T_{reg} recipients (**d-f**). Data representative of two independent experiments. Unpaired two-tailed Student's *t* test (**c-f**). Data are mean \pm s.e.m.

indicated conditions for 16 h in vitro. $n = 4$ technical replicates per condition; data are representative of three independent experiments. **d**, Representative flow cytometry showing gating (left) and replicate measurements (right) of CD45.2⁺ (transferred T_{reg}) and CD45.2⁻ (transferred T_{conv}) cells within the spleen and mesenteric lymph node of cell-transfer recipients. **e**, Replicate measurements of GARP expression on the indicated cell types from the spleen. **f**, Replicate measurements of expression of indicated cytokines by CD45.2⁻ T_{conv} cells from indicated tissues following brief restimulation ex vivo. $n = 5$ and 6, WT and Enh-KO T_{reg} recipients (**d-f**). Data representative of two independent experiments. Unpaired two-tailed Student's *t* test (**c-f**). Data are mean \pm s.e.m.

Article



Extended Data Fig. 10 | Conformational topography and eQTL analysis of human 11q13.5. **a**, Visualization of intrachromosomal interactions at human 11q13.5 within the B lymphoid line GM12878²⁹. A sub-topologically associated domain containing the identified enhancer and the promoter of *LRRK32* is indicated. Sample information and replicate statistics are in ref. ²⁹. **b**, Analysis of intrachromosomal H3K27ac-enriched HiChIP interactions in human CD4⁺ naive (CD45RA⁺CD25⁻CD127^{high}), T_{reg} (CD25⁺CD127^{low}), and T_{H17} cells (CD45RA⁻CD25⁻CD127^{high}CCR6⁺CXCR5⁺) isolated directly from human peripheral blood.

Sample information and replicate statistics are in ref. ²⁸. **c**, Expression quantitative trait locus (eQTL) analysis of the association between genetic polymorphisms at the indicated SNP with *LRRK32* expression in human CD4⁺CD127⁻CD25⁺ T_{reg} cells isolated by FACS from the blood of 123 healthy human donors. Point colours reflect linkage disequilibrium (R^2) relative to rs11236797. Nominal P value and FDR of the most significantly associated SNP are shown; linear regression, two-sided.

Reporting Summary

Nature Research wishes to improve the reproducibility of the work that we publish. This form provides structure for consistency and transparency in reporting. For further information on Nature Research policies, see [Authors & Referees](#) and the [Editorial Policy Checklist](#).

Statistics

For all statistical analyses, confirm that the following items are present in the figure legend, table legend, main text, or Methods section.

n/a Confirmed

- The exact sample size (n) for each experimental group/condition, given as a discrete number and unit of measurement
- A statement on whether measurements were taken from distinct samples or whether the same sample was measured repeatedly
- The statistical test(s) used AND whether they are one- or two-sided
Only common tests should be described solely by name; describe more complex techniques in the Methods section.
- A description of all covariates tested
- A description of any assumptions or corrections, such as tests of normality and adjustment for multiple comparisons
- A full description of the statistical parameters including central tendency (e.g. means) or other basic estimates (e.g. regression coefficient) AND variation (e.g. standard deviation) or associated estimates of uncertainty (e.g. confidence intervals)
- For null hypothesis testing, the test statistic (e.g. F , t , r) with confidence intervals, effect sizes, degrees of freedom and P value noted
Give P values as exact values whenever suitable.
- For Bayesian analysis, information on the choice of priors and Markov chain Monte Carlo settings
- For hierarchical and complex designs, identification of the appropriate level for tests and full reporting of outcomes
- Estimates of effect sizes (e.g. Cohen's d , Pearson's r), indicating how they were calculated

Our web collection on [statistics for biologists](#) contains articles on many of the points above.

Software and code

Policy information about [availability of computer code](#)

Data collection

Raw uncompensated flow cytometry data was acquired on BD Fortessa or BD LSRII instruments and exported as FCS files using BD FACSDiva software. Alternatively, high-parameter flow cytometry analysis was performed on a Propel Labs YETI (Bio-Rad ZE5). Data were compensated and analysed as described below.

RNA-sequencing libraries were prepared as described in the Methods section of the manuscript and sequenced using a HiSeq 2500 instrument (Illumina) and base calls were acquired using standard Illumina run-time analysis software and stored as FastQ files.

To obtain human SNP genotyping information, genomic DNA extracted from blood samples of 135 healthy European individuals were subjected to genotyping using the Infinium® CoreExome-24 v1.1 BeadChip (Illumina) and run on iScan System (Illumina).

Data analysis

Raw uncompensated flow cytometry data, exported as FCS files, were compensated using compensation controls acquired during each acquisition, and analysed using FlowJo v10.0 (Treestar).

Unaligned RNA-seq reads were trimmed using Trim Galore v0.4.4 using default parameters to remove the Nextera adapter sequence. Mapping was performed using HISAT2 v2.1.0 against the mouse NCBIM37 genome, guided by gene models from Ensembl annotation release 68. Aligned fragments were imported into SeqMonk (v1.44.0) and filtered to remove mappings with MAPQ scores of <20. Differential gene expression analysis was performed using the DESeq2 algorithm within SeqMonk.

Genotyping data were imputed using the 1000 Genomes Phase 3 reference panel and BEAGLE 4.16. After sequencing data quality control, regulatory peaks were called using MACS2. Gene and peak read counts were obtained using featureCounts. In each genomic layer were evaluated using linear models with QTLtools. Principal components that explained up to 1% of the observed variance per assay were included as covariates.

For manuscripts utilizing custom algorithms or software that are central to the research but not yet described in published literature, software must be made available to editors/reviewers. We strongly encourage code deposition in a community repository (e.g. GitHub). See the Nature Research [guidelines for submitting code & software](#) for further information.

Data

Policy information about [availability of data](#)

All manuscripts must include a [data availability statement](#). This statement should provide the following information, where applicable:

- Accession codes, unique identifiers, or web links for publicly available datasets
- A list of figures that have associated raw data
- A description of any restrictions on data availability

Data for RNA-Seq (Figure 2a, Supplementary Fig 6b, and Supplementary Table 2) and ATAC-Seq (Supplementary Fig 6a) analyses are deposited in GEO (accession GSE128198).

Data for human H3K27Ac hQTL and eQTL analyses (Figure 4a-c and Supplementary Fig 11c) are deposited in EGA (study accession EGAS00001003516, datasets EGAD00001004828 and EGAD00001004830).

Where analyses of previously published high-throughput sequencing-based data from other studies have been presented study references are provided in the Figure Legends which contain relevant sample information, replicate statistics and links to associated GEO accession numbers.

Field-specific reporting

Please select the one below that is the best fit for your research. If you are not sure, read the appropriate sections before making your selection.

Life sciences Behavioural & social sciences Ecological, evolutionary & environmental sciences

For a reference copy of the document with all sections, see nature.com/documents/nr-reporting-summary-flat.pdf

Life sciences study design

All studies must disclose on these points even when the disclosure is negative.

Sample size	Where relevant, sample sizes were determined using power calculations based on variability observed in prior experiments of a similar kind. In some experiments prior experience of sample size requirement was used to design experimental group sizes. For experiments where technical limitations prevented adequate statistical power to be obtained from single experiments, results from multiple experiments were pooled to provide sufficient statistical power.
Data exclusions	Flow cytometry samples which had undergone technical failure during processing or which had insufficient numbers of cells within relevant lymphocyte gates were excluded from analyses. Pre-established exclusion criteria across samples from a given experiment were used to avoid subjective bias. Experiments included positive and negative controls to allow technical failure of experiments to be objectively determined.
Replication	The number of independently repeated experiments for each finding are described in the figure legends. All technically successful replicate experiments reproduced the indicated findings.
Randomization	Data reported are in most cases non-subjective and did not require randomisation or blinding at measurement. Where appropriate, experimental cohorts were composed of randomised age- and sex-matched animals or subject to random Mendelian segregation of genotypes within litters.
Blinding	Investigators were not formally blinded. However, in randomised experiments it was difficult for investigators and technicians to readily determine genotypes from animal IDs at the bench.

Reporting for specific materials, systems and methods

We require information from authors about some types of materials, experimental systems and methods used in many studies. Here, indicate whether each material, system or method listed is relevant to your study. If you are not sure if a list item applies to your research, read the appropriate section before selecting a response.

Materials & experimental systems

n/a	Involved in the study
<input type="checkbox"/>	<input checked="" type="checkbox"/> Antibodies
<input type="checkbox"/>	<input checked="" type="checkbox"/> Eukaryotic cell lines
<input checked="" type="checkbox"/>	<input type="checkbox"/> Palaeontology
<input type="checkbox"/>	<input checked="" type="checkbox"/> Animals and other organisms
<input type="checkbox"/>	<input checked="" type="checkbox"/> Human research participants
<input checked="" type="checkbox"/>	<input type="checkbox"/> Clinical data

Methods

n/a	Involved in the study
<input type="checkbox"/>	<input checked="" type="checkbox"/> ChIP-seq
<input type="checkbox"/>	<input checked="" type="checkbox"/> Flow cytometry
<input checked="" type="checkbox"/>	<input type="checkbox"/> MRI-based neuroimaging

Antibodies

Antibodies used

Anti-mouse monoclonal antibodies with current lot numbers:

anti-GARP, Clone YGIC86, PE, 1:200, eBioscience Ref #12-9891-82, Lot 4310929
 anti-FoxP3, Clone FJK-16s, APC, 1:200, eBioscience Ref #17-5773-82, Lot 2013484
 anti-CD45.2, Clone 104, ef506, 1:200, eBioscience Ref #69-0454-82, Lot 4306084
 anti-TNF, Clone MP-XT22, PECy7, 1:200, eBioscience Ref #25-7321-82, Lot 4325990
 anti-IFN- γ , Clone XMG1.2, PerCP Cy5.5, 1:200, eBioscience Ref #45-7311-82, Lot 4321786
 anti-GL7, Clone GL7, FITC, 1:200, BioLegend Cat# 144604, Lot B184238
 anti-CD25, Clone PC61, BV786, 1:200, BD Cat# 564023, Lot 7240633
 anti-CD4, Clone RM4-5, ef450, 1:200, eBioscience, Ref #48-0042-82, Lot 1967921
 anti-CD62L, Clone MEL-14; BV510, 1:200, BioLegend, Cat #104441, Lot B259984
 anti-CD44, Clone IM7, FITC, 1:200, eBioscience, Ref #553133, Lot 24789
 anti-CD8a, Clone 53-6.7, BUV395 1:200, BD Horizon, Cat #563786, Lot 9164904
 anti-CD19, Clone eBio1D3, APC, 1:200, eBioscience, Ref #17-0193-80, Lot 4329179
 anti-B220, Clone RA3-6B2, PerCP Cy5.5, 1:200, eBioscience, Ref #103236, Lot B239431
 anti-TCRgd, Clone GL3, biotin, 1:400, eBioscience Ref #13-5711-85, Lot 4335132
 anti-CD11b, Clone M1/70, ef450, 1:200, eBioscience Ref #48-0112-82, Lot E10253-1632
 anti-CD90.2, Clone 53-2.1, BV510, 1:400, Biolegend Cat #105335, Lot B257116
 anti-CD11c, Clone N418, BV605, 1:400, Biolegend Cat #117334, Lot B280070
 anti-Ly6G, Clone 1A8, BV650, 1:200, Biolegend Cat #127641, Lot B260844
 anti-Ly6C, Clone HK1.4, BV711, 1:200, Biolegend Cat #128037, Lot B229095
 anti-Foxp3, Clone FJK-16s, AF488, 1:200, eBioscience Ref #53-5773-82, Lot 2068006
 anti-Siglec F, Clone E50-2440, PerCP-Cy5.5, 1:200, BD Bioscience Cat #565526, Lot 8232650
 anti-TCRb, Clone H57-597, BB790, 1:200, BD Bioscience, Cat #624296, Lot 8038906
 anti-F4/80, Clone BM8, PE-Cy5, 1:200, eBioscience Ref #15-4801-82, Lot 2100315
 anti-CD3, Clone 145.2C11, PE-Cy7, 1:200, eBioscience Ref #25-0031-82, Lot 4304567
 anti-CD45, Clone 30-F11, BUV395, 1:400, BD Bioscience Cat #564279, Lot 9016570
 anti-CD4, Clone GK1.5, BUV496, 1:200, BD Bioscience Cat #564667, Lot 9154927
 anti-CD19, Clone 1D3, BUV661, 1:200, BD Bioscience Cat #612971, Lot 9086987
 anti-PDCA-1, Clone 927, BUV737, 1:200, BD Bioscience Cat #749272, Lot 9114946
 anti-CD8a, Clone 53-6.7, APC, 1:200, eBioscience Ref #17-0081-83, Lot E07057-1635
 anti-MHCII (I-A/I-E), Clone M5/114.15.2, AF700, 1:200, eBioscience Ref #56-5321-82, Lot 2088410
 anti-NK1.1, Clone PK136, purified, 1:200, Biolegend Cat #108702, Lot unavailable
 anti-CD16/32, Clone 2.4G2, unconjugated, Cat #BE0307, Lot unavailable
 anti-CD28, Clone 37.51, unconjugated, BioXcell Cat #BE0015-1, Lot unavailable
 anti-CD3 Clone 145.2C11, unconjugated, BioXcell Cat #BE0001-1, Lot unavailable

Anti-human monoclonal antibodies with current lot numbers:

anti-CD3, Clone UCHT1, BUV395, 1:200, BD Horizon, Cat #563546, Lot 6343984
 anti-CD4, Clone SK3, PerCP Cy5.5, 1:400, BioLegend, Cat #344608, Lot B267675
 anti-CD127, Clone A019DS, PECy7, 1:200, BioLegend, Cat #351320, Lot B276187
 anti-CD25, Clone BC96, BV605, 1:200, BioLegend, Cat #302632, Lot B263590
 anti-GARP, Clone G14D9, PE, 1:200, eBioscience, Ref #12-9882-42, Lot 4311952
 anti-CD3 Clone OKT3, unconjugated, BioXcell Cat #BE0001-2, Lot unavailable
 anti-CD28 Clone 9.3, unconjugated, BioXcell Cat #BE0248, Lot unavailable

Validation

Antibody validation information is available for each of the listed antibodies on the relevant manufacturer website.

Eukaryotic cell lines

Policy information about [cell lines](#)

Cell line source(s)

HEK293T cells were obtained from ATCC

Authentication

No cell line authentication was performed; Low passage stocks were used

Mycoplasma contamination

Cell lines were screened for mycoplasma and found to be negative prior to use.

Commonly misidentified lines (See [ICLAC](#) register)

No commonly misidentified cell lines were used.

Animals and other organisms

Policy information about [studies involving animals; ARRIVE guidelines](#) recommended for reporting animal research

Laboratory animals

Mice used throughout the study were on C57BL/6 background. Unless otherwise specified in the manuscript, experiments were performed on 8-12 week old animals at the time of initiation of each experiment. Experimental and control groups comprised littermates or sex-matched male and female mice with an age range not exceeding 4 weeks.

Wild animals

Wild animals were not used in this study

Field-collected samples	The study did not involve samples collected from the field
Ethics oversight	All animal experiments were conducted in accordance with UK Home Office guidelines and were approved by the Babraham Institute Animal Welfare and Ethics Review Board.

Note that full information on the approval of the study protocol must also be provided in the manuscript.

Human research participants

Policy information about [studies involving human research participants](#)

Population characteristics	Leukodepletion cones for hQTL and eQTL analyses were obtained from healthy adults of Caucasian origin. For all donors we were able to determine sex based on their genotype and for 113 of the 123 donors we had access to age information. The majority of donors (78%) were genetically assigned males and were over 57 years old.
Recruitment	Leukocyte cones were obtained with informed consent from donors at the NHS Blood and Transplant, Cambridge (REC 15/NW/0282) and from the NHS Blood and Transplant, Oxford (REC 15/NS/0060). PBMC for experiments in Fig 4e were obtained with approval from healthy donors at New York Blood Center, New York, NY. PBMC samples for experiments in Fig. 4f were obtained from healthy donors at Policlinico San Matteo Pavia Fondazione IRCCS with ethical approval from Humanitas Research Hospital (date of approval 28.01.2016).
Ethics oversight	The study has been reviewed and approved by Research Ethics Committee and Institutional Human Materials and Data Management Committee.

Note that full information on the approval of the study protocol must also be provided in the manuscript.

ChIP-seq

Data deposition

- Confirm that both raw and final processed data have been deposited in a public database such as [GEO](#).
- Confirm that you have deposited or provided access to graph files (e.g. BED files) for the called peaks.

Data access links <i>May remain private before publication.</i>	Human H3K27Ac ChIP-Seq data are deposited in EGA (study accession EGAS00001003516) and contain the following files.
--	---

Files in database submission	file	sample_acc	sample_name	study_id
	25009_4#55.cram	EGAN00002036514	Treg_ChM7181889	5063
	24918_1#12.cram	EGAN00002036713	Treg_ChM7182088	5063
	25035_4#19.cram	EGAN00002036510	Treg_ChM7181885	5063
	25026_7#24.cram	EGAN00002036714	Treg_ChM7182089	5063
	25093_7#66.cram	EGAN00002036727	Treg_ChM7182102	5063
	25009_7#90.cram	EGAN00002036500	Treg_ChM7181875	5063
	25010_5#42.cram	EGAN00002036601	Treg_ChM7181976	5063
	25009_5#79.cram	EGAN00002036511	Treg_ChM7181886	5063
	25093_7#77.cram	EGAN00002036723	Treg_ChM7182098	5063
	25093_8#35.cram	EGAN00002036716	Treg_ChM7182091	5063
	25009_1#50.cram	EGAN00002036474	Treg_ChM7181849	5063
	24918_1#82.cram	EGAN00002036656	Treg_ChM7182031	5063
	25036_1#17.cram	EGAN00002036590	Treg_ChM7181965	5063
	25009_1#94.cram	EGAN00002036548	Treg_ChM7181923	5063
	25009_5#52.cram	EGAN00002036490	Treg_ChM7181865	5063
	25035_6#59.cram	EGAN00002036522	Treg_ChM7181897	5063
	25036_2#48.cram	EGAN00002036562	Treg_ChM7181937	5063
	25093_2#66.cram	EGAN00002036727	Treg_ChM7182102	5063
	25035_4#69.cram	EGAN00002036547	Treg_ChM7181922	5063
	25035_4#52.cram	EGAN00002036490	Treg_ChM7181865	5063
	25010_1#91.cram	EGAN00002036612	Treg_ChM7181987	5063
	25036_7#52.cram	EGAN00002036594	Treg_ChM7181969	5063
	25467_8#10.cram	EGAN00002036645	Treg_ChM7182020	5063
	25026_5#29.cram	EGAN00002036684	Treg_ChM7182059	5063
	25035_1#31.cram	EGAN00002036512	Treg_ChM7181887	5063
	24918_1#2.cram	EGAN00002036657	Treg_ChM7182032	5063
	25035_8#59.cram	EGAN00002036522	Treg_ChM7181897	5063
	25035_2#8.cram	EGAN00002036533	Treg_ChM7181908	5063
	25026_4#37.cram	EGAN00002036661	Treg_ChM7182036	5063
	25026_8#43.cram	EGAN00002036725	Treg_ChM7182100	5063
	25010_1#84.cram	EGAN00002036580	Treg_ChM7181955	5063
	25009_3#29.cram	EGAN00002036496	Treg_ChM7181871	5063
	25467_1#6.cram	EGAN00002036501	Treg_ChM7181876	5063
	25093_5#85.cram	EGAN00002036680	Treg_ChM7182055	5063
	25093_8#33.cram	EGAN00002036732	Treg_ChM7182107	5063
	25026_6#49.cram	EGAN00002036662	Treg_ChM7182037	5063

25035_7#3.cram	EGAN00002036477	Treg_ChM7181852	5063
25009_5#66.cram	EGAN00002036507	Treg_ChM7181882	5063
25036_3#49.cram	EGAN00002036570	Treg_ChM7181945	5063
25010_8#16.cram	EGAN00002036582	Treg_ChM7181957	5063
25467_8#73.cram	EGAN00002036591	Treg_ChM7181966	5063
25026_4#80.cram	EGAN00002036715	Treg_ChM7182090	5063
25093_2#13.cram	EGAN00002036650	Treg_ChM7182025	5063
25467_7#76.cram	EGAN00002036631	Treg_ChM7182006	5063
25093_8#4.cram	EGAN00002036673	Treg_ChM7182048	5063
25010_7#74.cram	EGAN00002036591	Treg_ChM7181966	5063
25467_8#76.cram	EGAN00002036631	Treg_ChM7182006	5063
25036_2#85.cram	EGAN00002036588	Treg_ChM7181963	5063
25035_8#33.cram	EGAN00002036544	Treg_ChM7181919	5063
25093_2#34.cram	EGAN00002036708	Treg_ChM7182083	5063
25036_5#19.cram	EGAN00002036606	Treg_ChM7181981	5063
25009_1#57.cram	EGAN00002036546	Treg_ChM7181921	5063
25026_8#63.cram	EGAN00002036687	Treg_ChM7182062	5063
25010_8#36.cram	EGAN00002036624	Treg_ChM7181999	5063
25026_4#27.cram	EGAN00002036668	Treg_ChM7182043	5063
25035_1#7.cram	EGAN00002036509	Treg_ChM7181884	5063
25010_7#49.cram	EGAN00002036570	Treg_ChM7181945	5063
25026_6#29.cram	EGAN00002036684	Treg_ChM7182059	5063
25009_6#66.cram	EGAN00002036507	Treg_ChM7181882	5063
25009_2#30.cram	EGAN00002036504	Treg_ChM7181879	5063
25035_5#51.cram	EGAN00002036482	Treg_ChM7181857	5063
25026_4#28.cram	EGAN00002036676	Treg_ChM7182051	5063
25036_1#79.cram	EGAN00002036615	Treg_ChM7181990	5063
25035_1#43.cram	EGAN00002036513	Treg_ChM7181888	5063
25035_7#11.cram	EGAN00002036517	Treg_ChM7181892	5063
25026_4#84.cram	EGAN00002036672	Treg_ChM7182047	5063
25035_8#28.cram	EGAN00002036488	Treg_ChM7181863	5063
25035_1#20.cram	EGAN00002036534	Treg_ChM7181909	5063
25010_6#66.cram	EGAN00002036635	Treg_ChM7182010	5063
25010_3#15.cram	EGAN00002036574	Treg_ChM7181949	5063
25093_6#25.cram	EGAN00002036652	Treg_ChM7182027	5063
25035_5#36.cram	EGAN00002036528	Treg_ChM7181903	5063
25026_5#27.cram	EGAN00002036668	Treg_ChM7182043	5063
25036_6#63.cram	EGAN00002036595	Treg_ChM7181970	5063
25036_5#21.cram	EGAN00002036638	Treg_ChM7182013	5063
25093_3#40.cram	EGAN00002036685	Treg_ChM7182060	5063
25010_3#5.cram	EGAN00002036589	Treg_ChM7181964	5063
25026_8#86.cram	EGAN00002036688	Treg_ChM7182063	5063
25009_5#59.cram	EGAN00002036522	Treg_ChM7181897	5063
25467_3#6.cram	EGAN00002036501	Treg_ChM7181876	5063
25009_1#73.cram	EGAN00002036463	Treg_ChM7181838	5063
25093_2#76.cram	EGAN00002036699	Treg_ChM7182074	5063
25093_1#63.cram	EGAN00002036687	Treg_ChM7182062	5063
25010_5#63.cram	EGAN00002036595	Treg_ChM7181970	5063
25009_7#20.cram	EGAN00002036534	Treg_ChM7181909	5063
25010_1#87.cram	EGAN00002036604	Treg_ChM7181979	5063
25035_6#85.cram	EGAN00002036460	Treg_ChM7181835	5063
25093_6#72.cram	EGAN00002036667	Treg_ChM7182042	5063
24918_1#46.cram	EGAN00002036709	Treg_ChM7182084	5063
25093_7#72.cram	EGAN00002036667	Treg_ChM7182042	5063
25035_4#12.cram	EGAN00002036525	Treg_ChM7181900	5063
25093_5#34.cram	EGAN00002036708	Treg_ChM7182083	5063
25026_8#29.cram	EGAN00002036684	Treg_ChM7182059	5063
25036_4#1.cram	EGAN00002036557	Treg_ChM7181932	5063
25009_3#68.cram	EGAN00002036539	Treg_ChM7181914	5063
25035_4#2.cram	EGAN00002036469	Treg_ChM7181844	5063
25035_8#35.cram	EGAN00002036520	Treg_ChM7181895	5063
25026_2#9.cram	EGAN00002036737	Treg_ChM7182112	5063
25026_7#78.cram	EGAN00002036731	Treg_ChM7182106	5063
25093_5#40.cram	EGAN00002036685	Treg_ChM7182060	5063
25093_7#5.cram	EGAN00002036681	Treg_ChM7182056	5063
25010_4#52.cram	EGAN00002036594	Treg_ChM7181969	5063
25026_7#55.cram	EGAN00002036726	Treg_ChM7182101	5063
25026_4#10.cram	EGAN00002036729	Treg_ChM7182104	5063
25010_7#9.cram	EGAN00002036637	Treg_ChM7182012	5063
25026_4#58.cram	EGAN00002036718	Treg_ChM7182093	5063
25010_2#56.cram	EGAN00002036642	Treg_ChM7182017	5063
25009_3#84.cram	EGAN00002036527	Treg_ChM7181902	5063
25036_4#37.cram	EGAN00002036561	Treg_ChM7181936	5063
25093_3#24.cram	EGAN00002036714	Treg_ChM7182089	5063
25467_1#65.cram	EGAN00002036499	Treg_ChM7181874	5063

25035_7#67.cram	EGAN00002036515	Treg_ChM7181890	5063
25093_3#29.cram	EGAN00002036684	Treg_ChM7182059	5063
25036_2#88.cram	EGAN00002036628	Treg_ChM7182003	5063
25026_3#13.cram	EGAN00002036650	Treg_ChM7182025	5063
25467_2#21.cram	EGAN00002036542	Treg_ChM7181917	5063
25035_8#9.cram	EGAN00002036541	Treg_ChM7181916	5063
25035_4#87.cram	EGAN00002036476	Treg_ChM7181851	5063
25035_8#11.cram	EGAN00002036517	Treg_ChM7181892	5063
25035_3#11.cram	EGAN00002036517	Treg_ChM7181892	5063
25026_3#38.cram	EGAN00002036669	Treg_ChM7182044	5063
25035_3#56.cram	EGAN00002036538	Treg_ChM7181913	5063
25010_1#33.cram	EGAN00002036640	Treg_ChM7182015	5063
25093_4#78.cram	EGAN00002036731	Treg_ChM7182106	5063
25010_6#37.cram	EGAN00002036561	Treg_ChM7181936	5063
25467_7#37.cram	EGAN00002036569	Treg_ChM7181944	5063
25026_6#15.cram	EGAN00002036666	Treg_ChM7182041	5063
25467_1#85.cram	EGAN00002036460	Treg_ChM7181835	5063
25035_8#38.cram	EGAN00002036473	Treg_ChM7181848	5063
25010_6#39.cram	EGAN00002036577	Treg_ChM7181952	5063
25010_4#67.cram	EGAN00002036643	Treg_ChM7182018	5063
25035_2#14.cram	EGAN00002036470	Treg_ChM7181845	5063
25467_1#86.cram	EGAN00002036468	Treg_ChM7181843	5063
25093_5#62.cram	EGAN00002036679	Treg_ChM7182054	5063
25036_7#42.cram	EGAN00002036601	Treg_ChM7181976	5063
25026_8#46.cram	EGAN00002036709	Treg_ChM7182084	5063
25093_1#15.cram	EGAN00002036666	Treg_ChM7182041	5063
24918_1#52.cram	EGAN00002036686	Treg_ChM7182061	5063
25093_7#76.cram	EGAN00002036699	Treg_ChM7182074	5063
25026_6#36.cram	EGAN00002036653	Treg_ChM7182028	5063
25026_2#30.cram	EGAN00002036692	Treg_ChM7182067	5063
25009_6#14.cram	EGAN00002036470	Treg_ChM7181845	5063
25010_6#53.cram	EGAN00002036602	Treg_ChM7181977	5063
25009_7#81.cram	EGAN00002036543	Treg_ChM7181918	5063
25009_5#90.cram	EGAN00002036500	Treg_ChM7181875	5063
25035_6#67.cram	EGAN00002036515	Treg_ChM7181890	5063
25010_7#60.cram	EGAN00002036571	Treg_ChM7181946	5063
25026_6#75.cram	EGAN00002036691	Treg_ChM7182066	5063
25026_5#91.cram	EGAN00002036704	Treg_ChM7182079	5063
25009_3#73.cram	EGAN00002036463	Treg_ChM7181838	5063
25467_7#15.cram	EGAN00002036582	Treg_ChM7181957	5063
25010_6#23.cram	EGAN00002036614	Treg_ChM7181989	5063
25035_3#66.cram	EGAN00002036507	Treg_ChM7181882	5063
25009_8#38.cram	EGAN00002036473	Treg_ChM7181848	5063
25035_5#64.cram	EGAN00002036491	Treg_ChM7181866	5063
25035_2#73.cram	EGAN00002036463	Treg_ChM7181838	5063
25026_5#46.cram	EGAN00002036709	Treg_ChM7182084	5063
25009_4#84.cram	EGAN00002036527	Treg_ChM7181902	5063
25026_6#55.cram	EGAN00002036726	Treg_ChM7182101	5063
25467_8#34.cram	EGAN00002036616	Treg_ChM7181991	5063
25036_3#91.cram	EGAN00002036612	Treg_ChM7181987	5063
25035_5#30.cram	EGAN00002036504	Treg_ChM7181879	5063
25010_5#9.cram	EGAN00002036637	Treg_ChM7182012	5063
25036_6#49.cram	EGAN00002036570	Treg_ChM7181945	5063
24911_1#53.cram	EGAN00002036602	Treg_ChM7181977	5063
24917_1#11.cram	EGAN00002036517	Treg_ChM7181892	5063
25036_2#22.cram	EGAN00002036646	Treg_ChM7182021	5063
25035_7#57.cram	EGAN00002036546	Treg_ChM7181921	5063
25026_5#41.cram	EGAN00002036693	Treg_ChM7182068	5063
24911_1#41.cram	EGAN00002036593	Treg_ChM7181968	5063
24918_1#63.cram	EGAN00002036687	Treg_ChM7182062	5063
25467_2#95.cram	EGAN00002036516	Treg_ChM7181891	5063
25010_8#41.cram	EGAN00002036593	Treg_ChM7181968	5063
25009_3#95.cram	EGAN00002036516	Treg_ChM7181891	5063
25035_2#9.cram	EGAN00002036541	Treg_ChM7181916	5063
25093_5#71.cram	EGAN00002036659	Treg_ChM7182034	5063
25009_5#25.cram	EGAN00002036464	Treg_ChM7181839	5063
25035_2#71.cram	EGAN00002036523	Treg_ChM7181898	5063
25036_7#24.cram	EGAN00002036622	Treg_ChM7181997	5063
25010_3#9.cram	EGAN00002036637	Treg_ChM7182012	5063
25036_2#79.cram	EGAN00002036615	Treg_ChM7181990	5063
25467_8#30.cram	EGAN00002036608	Treg_ChM7181983	5063
25026_3#37.cram	EGAN00002036661	Treg_ChM7182036	5063
25093_2#25.cram	EGAN00002036652	Treg_ChM7182027	5063
25026_5#9.cram	EGAN00002036737	Treg_ChM7182112	5063
25009_8#8.cram	EGAN00002036533	Treg_ChM7181908	5063

25093_3#43.cram	EGAN00002036725	Treg_ChM7182100	5063
25035_1#77.cram	EGAN00002036495	Treg_ChM7181870	5063
25035_5#46.cram	EGAN00002036553	Treg_ChM7181928	5063
25009_8#36.cram	EGAN00002036528	Treg_ChM7181903	5063
24918_1#19.cram	EGAN00002036698	Treg_ChM7182073	5063
25036_7#87.cram	EGAN00002036604	Treg_ChM7181979	5063
25035_6#55.cram	EGAN00002036514	Treg_ChM7181889	5063
25026_8#8.cram	EGAN00002036721	Treg_ChM7182096	5063
25467_2#20.cram	EGAN00002036534	Treg_ChM7181909	5063
25467_3#32.cram	EGAN00002036536	Treg_ChM7181911	5063
25467_1#88.cram	EGAN00002036484	Treg_ChM7181859	5063
25467_1#34.cram	EGAN00002036552	Treg_ChM7181927	5063
25035_7#29.cram	EGAN00002036496	Treg_ChM7181871	5063
24917_1#71.cram	EGAN00002036523	Treg_ChM7181898	5063
25010_4#48.cram	EGAN00002036562	Treg_ChM7181937	5063
25035_7#81.cram	EGAN00002036543	Treg_ChM7181918	5063
25093_6#84.cram	EGAN00002036672	Treg_ChM7182047	5063
25010_1#30.cram	EGAN00002036600	Treg_ChM7181975	5063
25009_4#79.cram	EGAN00002036511	Treg_ChM7181886	5063
24917_1#35.cram	EGAN00002036520	Treg_ChM7181895	5063
25035_3#72.cram	EGAN00002036531	Treg_ChM7181906	5063
25467_8#43.cram	EGAN00002036633	Treg_ChM7182008	5063
25035_4#54.cram	EGAN00002036506	Treg_ChM7181881	5063
25010_6#88.cram	EGAN00002036628	Treg_ChM7182003	5063
25010_3#84.cram	EGAN00002036580	Treg_ChM7181955	5063
25026_6#87.cram	EGAN00002036696	Treg_ChM7182071	5063
25035_3#31.cram	EGAN00002036512	Treg_ChM7181887	5063
25036_5#90.cram	EGAN00002036644	Treg_ChM7182019	5063
25035_7#18.cram	EGAN00002036502	Treg_ChM7181877	5063
25010_8#76.cram	EGAN00002036607	Treg_ChM7181982	5063
25036_7#79.cram	EGAN00002036615	Treg_ChM7181990	5063
25035_6#16.cram	EGAN00002036486	Treg_ChM7181861	5063
24917_1#38.cram	EGAN00002036473	Treg_ChM7181848	5063
25035_2#19.cram	EGAN00002036510	Treg_ChM7181885	5063
25009_7#25.cram	EGAN00002036464	Treg_ChM7181839	5063
25036_3#88.cram	EGAN00002036628	Treg_ChM7182003	5063
25009_2#12.cram	EGAN00002036525	Treg_ChM7181900	5063
25026_7#13.cram	EGAN00002036650	Treg_ChM7182025	5063
25009_1#27.cram	EGAN00002036480	Treg_ChM7181855	5063
25026_4#75.cram	EGAN00002036691	Treg_ChM7182066	5063
25026_4#12.cram	EGAN00002036713	Treg_ChM7182088	5063
25009_3#86.cram	EGAN00002036468	Treg_ChM7181843	5063
25010_7#75.cram	EGAN00002036599	Treg_ChM7181974	5063
25467_8#41.cram	EGAN00002036601	Treg_ChM7181976	5063
25093_1#31.cram	EGAN00002036700	Treg_ChM7182075	5063
25035_6#14.cram	EGAN00002036470	Treg_ChM7181845	5063
25009_5#14.cram	EGAN00002036470	Treg_ChM7181845	5063
25009_4#85.cram	EGAN00002036460	Treg_ChM7181835	5063
25035_1#14.cram	EGAN00002036470	Treg_ChM7181845	5063
25035_4#85.cram	EGAN00002036460	Treg_ChM7181835	5063
25026_3#14.cram	EGAN00002036658	Treg_ChM7182033	5063
25036_7#67.cram	EGAN00002036643	Treg_ChM7182018	5063
24918_1#6.cram	EGAN00002036689	Treg_ChM7182064	5063
25467_8#23.cram	EGAN00002036622	Treg_ChM7181997	5063
25036_6#58.cram	EGAN00002036626	Treg_ChM7182001	5063
25010_2#73.cram	EGAN00002036583	Treg_ChM7181958	5063
25010_3#76.cram	EGAN00002036607	Treg_ChM7181982	5063
25010_1#79.cram	EGAN00002036615	Treg_ChM7181990	5063
25010_5#53.cram	EGAN00002036602	Treg_ChM7181977	5063
24911_1#32.cram	EGAN00002036632	Treg_ChM7182007	5063
25035_5#61.cram	EGAN00002036467	Treg_ChM7181842	5063
25035_7#49.cram	EGAN00002036466	Treg_ChM7181841	5063
25026_7#75.cram	EGAN00002036691	Treg_ChM7182066	5063
24911_1#19.cram	EGAN00002036606	Treg_ChM7181981	5063
25026_6#31.cram	EGAN00002036700	Treg_ChM7182075	5063
25009_7#68.cram	EGAN00002036539	Treg_ChM7181914	5063
25035_7#79.cram	EGAN00002036511	Treg_ChM7181886	5063
25010_2#30.cram	EGAN00002036600	Treg_ChM7181975	5063
24918_1#84.cram	EGAN00002036672	Treg_ChM7182047	5063
25026_4#55.cram	EGAN00002036726	Treg_ChM7182101	5063
24917_1#7.cram	EGAN00002036509	Treg_ChM7181884	5063
25035_4#62.cram	EGAN00002036475	Treg_ChM7181850	5063
25467_7#60.cram	EGAN00002036579	Treg_ChM7181954	5063
25093_5#69.cram	EGAN00002036719	Treg_ChM7182094	5063
25036_4#63.cram	EGAN00002036595	Treg_ChM7181970	5063

25010_8#83.cram	EGAN00002036572	Treg_ChM7181947	5063
25009_3#79.cram	EGAN00002036511	Treg_ChM7181886	5063
25467_7#46.cram	EGAN00002036625	Treg_ChM7182000	5063
25009_8#29.cram	EGAN00002036496	Treg_ChM7181871	5063
25036_5#17.cram	EGAN00002036590	Treg_ChM7181965	5063
24911_1#15.cram	EGAN00002036574	Treg_ChM7181949	5063
25026_8#76.cram	EGAN00002036699	Treg_ChM7182074	5063
25009_6#88.cram	EGAN00002036484	Treg_ChM7181859	5063
25026_2#71.cram	EGAN00002036659	Treg_ChM7182034	5063
25026_2#80.cram	EGAN00002036715	Treg_ChM7182090	5063
25009_7#39.cram	EGAN00002036481	Treg_ChM7181856	5063
25026_8#91.cram	EGAN00002036704	Treg_ChM7182079	5063
25010_3#90.cram	EGAN00002036644	Treg_ChM7182019	5063
25093_6#83.cram	EGAN00002036664	Treg_ChM7182039	5063
25036_3#16.cram	EGAN00002036582	Treg_ChM7181957	5063
25035_5#95.cram	EGAN00002036516	Treg_ChM7181891	5063
25010_7#51.cram	EGAN00002036586	Treg_ChM7181961	5063
25010_1#40.cram	EGAN00002036585	Treg_ChM7181960	5063
25036_4#34.cram	EGAN00002036647	Treg_ChM7182022	5063
25093_4#12.cram	EGAN00002036713	Treg_ChM7182088	5063
25093_2#16.cram	EGAN00002036674	Treg_ChM7182049	5063
25035_5#81.cram	EGAN00002036543	Treg_ChM7181918	5063
25026_4#68.cram	EGAN00002036711	Treg_ChM7182086	5063
25009_6#67.cram	EGAN00002036515	Treg_ChM7181890	5063
25036_3#39.cram	EGAN00002036577	Treg_ChM7181952	5063
25009_5#2.cram	EGAN00002036469	Treg_ChM7181844	5063
25467_2#11.cram	EGAN00002036517	Treg_ChM7181892	5063
25467_2#53.cram	EGAN00002036498	Treg_ChM7181873	5063
25026_8#6.cram	EGAN00002036689	Treg_ChM7182064	5063
25467_7#3.cram	EGAN00002036573	Treg_ChM7181948	5063
25026_7#52.cram	EGAN00002036686	Treg_ChM7182061	5063
25009_4#69.cram	EGAN00002036547	Treg_ChM7181922	5063
25467_2#56.cram	EGAN00002036538	Treg_ChM7181913	5063
25467_3#83.cram	EGAN00002036519	Treg_ChM7181894	5063
25093_7#33.cram	EGAN00002036732	Treg_ChM7182107	5063
25093_2#20.cram	EGAN00002036722	Treg_ChM7182097	5063
25010_4#79.cram	EGAN00002036615	Treg_ChM7181990	5063
25467_8#50.cram	EGAN00002036586	Treg_ChM7181961	5063
25010_7#35.cram	EGAN00002036616	Treg_ChM7181991	5063
25009_5#83.cram	EGAN00002036519	Treg_ChM7181894	5063
25467_3#92.cram	EGAN00002036532	Treg_ChM7181907	5063
25035_1#65.cram	EGAN00002036499	Treg_ChM7181874	5063
25035_6#19.cram	EGAN00002036510	Treg_ChM7181885	5063
25009_2#32.cram	EGAN00002036536	Treg_ChM7181911	5063
25467_3#29.cram	EGAN00002036496	Treg_ChM7181871	5063
25467_2#23.cram	EGAN00002036518	Treg_ChM7181893	5063
25036_6#90.cram	EGAN00002036644	Treg_ChM7182019	5063
25009_1#90.cram	EGAN00002036500	Treg_ChM7181875	5063
25026_4#73.cram	EGAN00002036675	Treg_ChM7182050	5063
25010_5#82.cram	EGAN00002036564	Treg_ChM7181939	5063
25010_3#3.cram	EGAN00002036573	Treg_ChM7181948	5063
25467_8#57.cram	EGAN00002036626	Treg_ChM7182001	5063
25010_1#63.cram	EGAN00002036595	Treg_ChM7181970	5063
25026_3#31.cram	EGAN00002036700	Treg_ChM7182075	5063
25467_1#73.cram	EGAN00002036463	Treg_ChM7181838	5063
25009_1#86.cram	EGAN00002036468	Treg_ChM7181843	5063
24918_1#45.cram	EGAN00002036733	Treg_ChM7182108	5063
25026_2#56.cram	EGAN00002036734	Treg_ChM7182109	5063
25010_8#70.cram	EGAN00002036559	Treg_ChM7181934	5063
25009_3#37.cram	EGAN00002036465	Treg_ChM7181840	5063
25467_3#96.cram	EGAN00002036524	Treg_ChM7181899	5063
25467_7#51.cram	EGAN00002036594	Treg_ChM7181969	5063
25036_1#31.cram	EGAN00002036608	Treg_ChM7181983	5063
25010_8#61.cram	EGAN00002036579	Treg_ChM7181954	5063
25009_3#38.cram	EGAN00002036473	Treg_ChM7181848	5063
25010_4#16.cram	EGAN00002036582	Treg_ChM7181957	5063
25010_8#48.cram	EGAN00002036562	Treg_ChM7181937	5063
25467_7#2.cram	EGAN00002036565	Treg_ChM7181940	5063
25035_4#40.cram	EGAN00002036489	Treg_ChM7181864	5063
25009_3#28.cram	EGAN00002036488	Treg_ChM7181863	5063
25010_5#89.cram	EGAN00002036636	Treg_ChM7182011	5063
25010_4#20.cram	EGAN00002036630	Treg_ChM7182005	5063
24917_1#81.cram	EGAN00002036543	Treg_ChM7181918	5063
25035_8#45.cram	EGAN00002036545	Treg_ChM7181920	5063
24917_1#52.cram	EGAN00002036490	Treg_ChM7181865	5063

25093_6#36.cram	EGAN00002036653	Treg_ChM7182028	5063
25009_4#35.cram	EGAN00002036520	Treg_ChM7181895	5063
25010_6#87.cram	EGAN00002036600	Treg_ChM7181979	5063
25009_3#19.cram	EGAN00002036510	Treg_ChM7181885	5063
25035_6#33.cram	EGAN00002036544	Treg_ChM7181919	5063
25010_2#10.cram	EGAN00002036645	Treg_ChM7182020	5063
25035_8#18.cram	EGAN00002036502	Treg_ChM7181877	5063
25009_7#96.cram	EGAN00002036524	Treg_ChM7181899	5063
24911_1#60.cram	EGAN00002036571	Treg_ChM7181946	5063
25010_3#34.cram	EGAN00002036647	Treg_ChM7182022	5063
25009_6#45.cram	EGAN00002036545	Treg_ChM7181920	5063
25009_2#6.cram	EGAN00002036501	Treg_ChM7181876	5063
25009_5#28.cram	EGAN00002036488	Treg_ChM7181863	5063
25035_3#96.cram	EGAN00002036524	Treg_ChM7181899	5063
25093_7#24.cram	EGAN00002036714	Treg_ChM7182089	5063
25026_8#55.cram	EGAN00002036726	Treg_ChM7182101	5063
25009_7#31.cram	EGAN00002036512	Treg_ChM7181887	5063
25009_1#64.cram	EGAN00002036491	Treg_ChM7181866	5063
25036_2#34.cram	EGAN00002036647	Treg_ChM7182022	5063
25035_4#18.cram	EGAN00002036502	Treg_ChM7181877	5063
25035_1#69.cram	EGAN00002036547	Treg_ChM7181922	5063
25035_1#54.cram	EGAN00002036506	Treg_ChM7181881	5063
25093_7#68.cram	EGAN00002036711	Treg_ChM7182086	5063
25036_6#61.cram	EGAN00002036579	Treg_ChM7181954	5063
24917_1#61.cram	EGAN00002036467	Treg_ChM7181842	5063
25036_3#59.cram	EGAN00002036563	Treg_ChM7181938	5063
24917_1#8.cram	EGAN00002036533	Treg_ChM7181908	5063
25093_3#45.cram	EGAN00002036733	Treg_ChM7182108	5063
25467_3#40.cram	EGAN00002036489	Treg_ChM7181864	5063
25035_2#45.cram	EGAN00002036545	Treg_ChM7181920	5063
25036_5#2.cram	EGAN00002036565	Treg_ChM7181940	5063
25010_7#85.cram	EGAN00002036588	Treg_ChM7181963	5063
25010_8#54.cram	EGAN00002036610	Treg_ChM7181985	5063
25010_3#19.cram	EGAN00002036606	Treg_ChM7181981	5063
25036_5#82.cram	EGAN00002036564	Treg_ChM7181939	5063
25467_8#81.cram	EGAN00002036572	Treg_ChM7181947	5063
25010_5#79.cram	EGAN00002036615	Treg_ChM7181990	5063
25036_1#86.cram	EGAN00002036596	Treg_ChM7181971	5063
25010_7#71.cram	EGAN00002036567	Treg_ChM7181942	5063
25467_8#45.cram	EGAN00002036617	Treg_ChM7181992	5063
25035_1#58.cram	EGAN00002036554	Treg_ChM7181929	5063
25010_2#27.cram	EGAN00002036576	Treg_ChM7181951	5063
25010_1#2.cram	EGAN00002036565	Treg_ChM7181940	5063
25467_8#62.cram	EGAN00002036595	Treg_ChM7181970	5063
25035_6#4.cram	EGAN00002036485	Treg_ChM7181860	5063
25035_2#91.cram	EGAN00002036508	Treg_ChM7181883	5063
25093_6#63.cram	EGAN00002036687	Treg_ChM7182062	5063
25010_7#59.cram	EGAN00002036563	Treg_ChM7181938	5063
24911_1#39.cram	EGAN00002036577	Treg_ChM7181952	5063
25010_6#49.cram	EGAN00002036570	Treg_ChM7181945	5063
25093_8#16.cram	EGAN00002036674	Treg_ChM7182049	5063
25026_6#22.cram	EGAN00002036730	Treg_ChM7182105	5063
25035_8#96.cram	EGAN00002036524	Treg_ChM7181899	5063
25009_8#87.cram	EGAN00002036476	Treg_ChM7181851	5063
25467_8#51.cram	EGAN00002036594	Treg_ChM7181969	5063
25036_7#92.cram	EGAN00002036620	Treg_ChM7181995	5063
25093_6#67.cram	EGAN00002036735	Treg_ChM7182110	5063
25093_6#27.cram	EGAN00002036668	Treg_ChM7182043	5063
25093_2#24.cram	EGAN00002036714	Treg_ChM7182089	5063
25010_6#19.cram	EGAN00002036600	Treg_ChM7181981	5063
25035_6#49.cram	EGAN00002036466	Treg_ChM7181841	5063
24917_1#54.cram	EGAN00002036506	Treg_ChM7181881	5063
24911_1#75.cram	EGAN00002036599	Treg_ChM7181974	5063
25467_8#29.cram	EGAN00002036600	Treg_ChM7181975	5063
25467_2#55.cram	EGAN00002036514	Treg_ChM7181889	5063
25009_4#7.cram	EGAN00002036509	Treg_ChM7181884	5063
25036_1#36.cram	EGAN00002036624	Treg_ChM7181999	5063
25035_7#35.cram	EGAN00002036520	Treg_ChM7181895	5063
25035_4#66.cram	EGAN00002036507	Treg_ChM7181882	5063
25467_3#90.cram	EGAN00002036500	Treg_ChM7181875	5063
24917_1#28.cram	EGAN00002036488	Treg_ChM7181863	5063
24911_1#12.cram	EGAN00002036621	Treg_ChM7181996	5063
24917_1#66.cram	EGAN00002036507	Treg_ChM7181882	5063
25009_5#18.cram	EGAN00002036502	Treg_ChM7181877	5063
24918_1#7.cram	EGAN00002036697	Treg_ChM7182072	5063

25036_1#27.cram	EGAN00002036576	Treg_ChM7181951	5063
25093_4#11.cram	EGAN00002036705	Treg_ChM7182080	5063
25009_8#66.cram	EGAN00002036507	Treg_ChM7181882	5063
25467_8#89.cram	EGAN00002036620	Treg_ChM7181995	5063
25026_3#9.cram	EGAN00002036737	Treg_ChM7182112	5063
24917_1#62.cram	EGAN00002036475	Treg_ChM7181850	5063
25093_4#82.cram	EGAN00002036656	Treg_ChM7182031	5063
25467_2#73.cram	EGAN00002036463	Treg_ChM7181838	5063
25036_4#10.cram	EGAN00002036645	Treg_ChM7182020	5063
25009_7#34.cram	EGAN00002036552	Treg_ChM7181927	5063
25036_6#33.cram	EGAN00002036640	Treg_ChM7182015	5063
25093_6#17.cram	EGAN00002036682	Treg_ChM7182057	5063
25467_8#52.cram	EGAN00002036602	Treg_ChM7181977	5063
25036_1#50.cram	EGAN00002036578	Treg_ChM7181953	5063
25036_4#66.cram	EGAN00002036635	Treg_ChM7182010	5063

Genome browser session
(e.g. [UCSC](#))

Provide a link to an anonymized genome browser session for "Initial submission" and "Revised version" documents only, to enable peer review. Write "no longer applicable" for "Final submission" documents.

Methodology

Replicates

29 technical replicates were performed to test technical variability; each donor constituted a biological replicate

Sequencing depth

Reads were trimmed using skewer. Trimmed reads were aligned to the GrCh38 assembly of the human genome using bwa (Li and Durbin, 2009) and employing the mem algorithm. Multi-mapping reads and duplicated reads were removed using samtools (Li et al., 2009). Only reads mapping to autosomes were maintained. A median of 40 million reads in the H3K27ac ChM-seq assays, passed this QC. We used paired-end sequencing

Antibodies

Cat. no. C15410196, Diagenode

Peak calling parameters

Prior to calling peaks from histone ChM-seq data, we merged a combined input reaching more than 223 million reads. In order to define a consensus set of peaks per chromatin assay, we performed a merged peak calling combining reads from all the donors. We downsampled each donor sample using samtools to 1.86 million read pairs per H3K27ac assay in order to reach similar read counts to the sequenced inputs. H3K27ac broad peaks were called using the standard broad peaks macs2 model and an adjusted p-value of 0.01, specifying -f BAMPE --broad --down-sample --broad-cutoff 0.1 -q 0.01. We used the MACS2 parameters described above and specifying --keep-dup all. Then, to ensure a sufficient number of reads per peak, only ATAC-seq peaks with at least 10 reads in 80% of the samples, and ChM-seq peaks with fold enrichment >= 2 and adjusted p-value < 0.001, were maintained in the final set. Genome browser data was constructed using the MACS2 -B flag and reads were normalised to signal per million.

Data quality

Samples with less than 10,000 peaks (median H3K27ac 68,626), fraction of reads in peaks (FRIP) lower than 10% (median H3K27ac 63.9%) were discarded. Additionally, the samples that did not cluster with the corresponding group in principal component analysis (considering log2 transformed number of reads in genomic bins of 10,000 bp, after normalization by library length) were discarded from further analysis. Finally, a total of 91 individuals passed these filters for H3K27ac samples.

Software

Read alignment: Fast and accurate short read alignment with Burrows-Wheeler transform. Li H, Durbin R. Bioinformatics, 2009
Read QC: The Sequence Alignment/Map format and SAMtools. Li H, Handsaker B, Wysoker A, Fennell T, Ruan J, Homer N, Marth G et al. Bioinformatics, 2009
Peak calling: Model-based Analysis of ChIP-Seq (MACS). Zhang Y, Liu T, Meyer CA, Eeckhoute J, Johnson DS, Bernstein BE et al. Genome Biol., 2008

Flow Cytometry

Plots

Confirm that:

- The axis labels state the marker and fluorochrome used (e.g. CD4-FITC).
- The axis scales are clearly visible. Include numbers along axes only for bottom left plot of group (a 'group' is an analysis of identical markers).
- All plots are contour plots with outliers or pseudocolor plots.
- A numerical value for number of cells or percentage (with statistics) is provided.

Methodology

Sample preparation

As described in the manuscript, Single-cell suspensions from lymphoid tissues were prepared by dissociating tissues over 40μm cell strainers. Lungs were minced in media containing 20 ug/ml DNase I (Roche) and 1 mg/ml collagenase (Sigma-Aldrich) and incubated with agitation at 37 °C for 30 minutes. Blood from tail veins or terminal cardiac bleeds were isolated in EDTA Microvette tubes (Sarstedt). Erythrocytes were lysed using ice cold ACK Lysing Buffer (Gibco) for 45 seconds. Cells requiring

intracellular staining of cytokines prior to flow cytometry analysis were stimulated using phorbol 12-myristate 13-acetate (PMA), ionomycin and brefeldin A (BFA) for 4-6h in complete media. Viable cells were discriminated by staining with Zombie UV live/dead dye (Biolegend) or eFluor 780 live/dead dye (eBioscience) according to manufacturer instructions. Cells were then incubated with specific antibodies for 30 min on ice in the presence of 2.4G2 monoclonal antibodies to block Fc γ R binding. For intracellular staining, the eBioscience Foxp3 / Transcription Factor Staining Buffer Set (Invitrogen) was used in accordance with manufacturers instructions followed by intracellular staining with fluorochrome-conjugated antibodies.

Instrument

Samples were analysed using BD LSRFortessa or LSR II instruments (Becton Dickinson Biosciences) and raw data was acquired and exported using BD FACSDiva software as FCS 3.0 files.

Software

FCS 3.0 files containing uncompensated flow cytometry data were compensated and analysed using FlowJo software (Treestar LLC). Cells were gated as described in the manuscript.

Cell population abundance

For FACS sorting experiments, pre-enriched CD4+ T cells were stained using flow cytometry cell surface antibodies. Cell sorting was performed using a BD Influx instrument (Becton Dickinson Biosciences). Cells were sorted into solutions of RPMI 1640 medium supplemented with 20% Fetal Bovine Serum (Sigma-Aldrich). Post-sort samples exceeding >95% purity were used for subsequent analysis. Purity as assessed by re-running post-sort samples through the FACS instrument and assessing the frequency of cells not falling within sort gates.

Gating strategy

In general, cells were gated based on a viability gate using amine-reactive viability exclusion dye intensity, a lymphocyte gate, a singlet gate and then subsequent gating based on the expression of surface and intracellular proteins as described in the manuscript.

Tick this box to confirm that a figure exemplifying the gating strategy is provided in the Supplementary Information.